Palaeogeography, Palaeoclimatology, Palaeoecology 669 (2025) 112907

Contents lists available at ScienceDirect

Palaeogeography, Palaeoclimatology, Palaeoecology

journal homepage: www.elsevier.com/locate/palaeo

Strontium-isotope stratigraphy: methodology, standard values (SRM987, EN-1, E&A), a new Neogene curve of $^{87}Sr/^{86}Sr$ against time, its implications for astrochronology ([I]ODP Sites 1146, 1264, U1337, and U1338), and its application to ODP Site 758 (Indian summer monsoon) and IODP Site 1120 (a new age-model)

J.M. McArthur [a,*], I.L. Millar [b], A.J. Drury [a,c,1], D. Wagner [b]

[a] Department of Earth Sciences, UCL, Gower Street, London WC1E 6BT, UK
[b] National Environmental Isotope Facility, British Geological Survey, Keyworth, Nottingham NG12 5GG, UK
[c] School of Geography, Geology and the Environment, University of Leicester, Leicester LE1 7RH, UK

ARTICLE INFO

Editor: Bing Shen

Keywords:
EN-1
SRM987
E&A
SIS
Sr-isotope
$^{87}Sr/^{86}Sr$
Neogene
Site 758
Site 1120
Site 1264
Site U1337
Site U1338
Indian summer monsoon

ABSTRACT

For the standards SRM(NIST) 987, EN-1, and E&A, we present compilations of $^{87}Sr/^{86}Sr$ from the literature, and 125 new measurements of $^{87}Sr/^{86}Sr$, to arrive at recommend values of 0.710 248, 0.709 172, and 0.708 021 respectively, for normalising $^{87}Sr/^{86}Sr$ data for use in Sr-isotope stratigraphy. Using these standards, interlaboratory comparison of $^{87}Sr/^{86}Sr$ data is, nevertheless, impaired by residual bias of up to 0.000 072 that is not removed by normalisation of $^{87}Sr/^{86}Sr$ data to accepted values for standards. We also provide a new reference curve of $^{87}Sr/^{86}Sr$ against time for the period 11 to 20 Ma that is based on high-precision (± 0.000 003, 2 s.e.) analysis of $^{8\,7}Sr/^{86}Sr$ in microfossil calcite from the ODP Sites 1146 and 1264, and IODP Sites U1337 and U1338. Ages for Site U1338 are calibrated by bio-magnetostratigraphy, whilst the others are calibrated by astrochronology, within which anomalies of up to 1.0 myrs are noted. With literature data, we extend the curve to 0 and 32 Ma. We show that the previous $^{87}Sr/^{86}Sr$ reference curve for the interval 0 – 7 Ma, that of Farrell et al. (1995) for Site 758 in the southern Bay of Bengal, is compromised by riverine influences from the Ganges/Brahmaputra rivers: differences between that curve and our new curve are interpreted to be a proxy for the intensity of the Indian summer monsoon. Finally, for Site 1120, a new age-model is presented, based on $^{87}Sr/^{86}Sr$, in order to test the biostratigraphic age-model for the site, which is found to be good. This work shows that integrated approaches to improving the chronological framework of Cenozoic successions should include Sr-isotope stratigraphy.

1. Introduction

In 1948, Frans Wickman suggested that the $^{87}Sr/^{86}Sr$ of Sr in the oceans had increased linearly through geologic time and proposed that that increase could be used to date marine precipitates, such as carbonate and gypsum (Wickman, 1948). Early tests of the suggestion (Peterman et al., 1970; Dasch and Biscaye, 1971; Veizer and Compston, 1974) showed a variable $^{87}Sr/^{86}Sr$ through time and not the linear increase suggested. Subsequent work led to the first Phanerozoic curve of marine-$^{87}Sr/^{86}Sr$ through time (Burke et al., 1982) and the first detailed Cenozoic curve (DePaolo and Ingram, 1985; DePaolo, 1986) for use in dating and for modelling exogenic cycles. Since then, numerous workers have improved the Cenozoic reference curve for use in Sr-isotope stratigraphy (SIS; Miller et al., 1988, 1991; Hodell et al., 1989, 1990, 1991; Oslick et al., 1994; Hodell and Woodruff, 1994, Mead and Hodell, 1995; Farrell et al., 1995; Martin et al., 1999; Reilly et al., 2002; McArthur et al., 2006; Ando et al., 2011).

In the decades since completion of the work cited above, improvements have occurred in the precision with which $^{87}Sr/^{86}Sr$ can be measured and in the ability to recover complete (spliced) cores of

* Corresponding author.
E-mail address: j.mcarthur@ucl.ac.uk (J.M. McArthur).
[1] Current Address

https://doi.org/10.1016/j.palaeo.2025.112907
Received 17 June 2024; Received in revised form 18 March 2025; Accepted 18 March 2025
Available online 19 March 2025

Fig. 1. Location of ODP/IODP Sites mentioned in this work. Base map from https://www.waterproofpaper.com/printable-maps/world.shtml
758. Northern Indian Ocean, Bay of Bengal. 5 ° 23.04′N, 90° 21.67′ E 2925 m. water depth.
1120. Campbell Plateau. 50° 3.82′ S, 173° 22.30′ E; 543 m. water depth.
1146. South China Sea. 19° 27.40′ N, 116° 16.37′ E; 2091 m. water depth.
1264. South-east Atlantic Ocean; Walvis Ridge. 28° 31.96′ S, 2° 50.73′ E
U1337. Equatorial Pacific Ocean. 3° 50.009′ N, 123° 12.352′ W; 4463 m. water depth.
U1338. Equatorial Pacific Ocean. 2° 30.469′ N, 117° 58.178′ W; 4200 m. water depth.

Cenozoic deep-sea sediments and accurately date them. We build on these improvements to revise the Neogene reference curve for $^{87}Sr/^{86}Sr$.

To anchor our curve to standards, we determined the best values of $^{87}Sr/^{86}Sr$ for the standards in use for SIS (SRM987, EN-1, and E&A) both by measurement and by statistical analysis of literature data. That process highlighted the problem of interlaboratory bias, and residual interlaboratory bias, the latter being the bias in measurement of $^{87}Sr/^{86}Sr$ between laboratories that remains *after* normalisation of $^{87}Sr/^{86}Sr$ to a common standard.

Having established the accuracy of our analysis, we then present a new curve for the interval 11 – 20 Ma, based on high-precision analysis for $^{87}Sr/^{86}Sr$ (± 0.000 003, 2 s.e.) in microfossils from the [I]ODP cores from Sites 1146, 1264, U1337, and U1338 (Fig. 1). Using the new curve, we revise the depth/age model for ODP Site 1120 (Fig. 1; Carter et al., 1999; Ando et al., 2011), the only other Neogene site with a high-precision (± 0.000 005) record of $^{87}Sr/^{86}Sr$ *versus* depth. We then extend the curve to 0 and 32 Ma using literature data, after suitable revision.

In doing the above, two difficulties were encountered. Firstly, in trends of $^{87}Sr/^{86}Sr$ against astrochronometric (CENOGRID) ages, data for Sites 1146 and U1338 are offset by up to 1.0 myrs and some data for Site 1264 appear anomalous by up to 0.24 myrs. We therefore developed local age models based on $^{87}Sr/^{86}Sr$ for these small intervals. The anomalies suggest that small parts of the depth-age models for Sites 1146, 1264, and U1338, need re-evaluation. Secondly, the previous $^{87}Sr/^{86}Sr$ curve for the interval 0 to 7 Ma, that of Farrell et al. (1995) based on ODP Site 758 in the Bay of Bengal (Fig. 1), appears to be biased by riverine influence from the Ganges and Brahmaputra rivers, both of which have exceptionally high $^{87}Sr/^{86}Sr$. That reference curve can no longer be considered reliable for SIS but has another value: differences between Farrell et al. (1995) and our new curve, which is based on open-ocean sites unaffected by river influence, are interpreted as showing changes in the intensity of the Indian summer monsoon.

These complexities have implications for the use of high-precision Sr-isotope stratigraphy (SIS). It can provide independent testing of other chronological approaches (*e.g.*, bio-magneto-chemo-stratigraphy; astrochronology) and should be incorporated within an integrated stratigraphic approach to test and improve marine chronology.

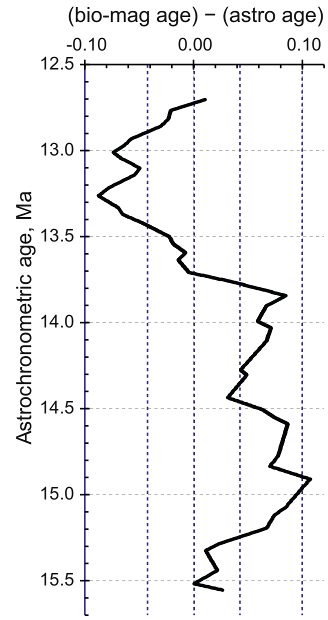

Fig. 2. For U1338, the difference is shown between the numeric ages given in the compilation by Holbourn et al. (2024) and those derived from the bio-magneto-stratigraphy of Backman et al. (2016). Dotted blue vertical lines are drawn at 41 kyrs and 100 kyrs from zero. The data used to construct this figure are in the Supplementary Information. (For interpretation of the references to colour in this figure legend, the reader is referred to the web version of this article.)

2. Samples and methods

2.1. Samples and Sites

To obtain our marine-$^{87}Sr/^{86}Sr$ curve for the interval 11 – 20 Ma, we analysed samples from deep-sea cores from Ocean Discovery Program (ODP) Sites 1146 (North China Sea) and 1264 (Southeast Atlantic), and Integrated Ocean Drilling Programme (IODP) Sites, U1337 and U1338 (Eastern Equatorial Pacific).

Depth and age models mostly follow CENOGRID (Westerhold et al., 2020) and are based on the following: Site 1146 composite depth (rmcd) from Holbourn et al. (2018) and astrochronology from De Vleeschouwer et al. (2020); Site 1264 composite depth (rmcd) from Drury et al. (2021) and astrochronology from Liebrand et al. (Liebrand et al., 2016; verified in Drury et al., 2021). For Site U1337, we use both CENOGRID ages and the age-depth model of Hilgen (2025). Of our twenty-three samples from U1337, only nine came from cores common to both us and Hilgen (2025), so only nine Hilgen-ages are directly available for U1337. Nevertheless, they spread over a useful age-range. To the age-depth models used, we made adjustments where necessary using a $^{87}Sr/^{86}Sr$-based chronology. Complementary ages from CENOGRID comprise the composite depths (rmcd) from Wilkens et al. (2013) including the minor revision from Lyle et al. (2019) and astrochronology by Kochhann et al. (2016) and Holbourn et al. (2015, 2022, 2024). For Site U1338, we use the bio-magneto-stratigraphic age calibration of Backman et al. (2016) rather than the astrocalibration used in CENOGRID because, despite close agreement (Fig. 2; data for this figure are in the Supplementary Infomation), the differences between the two is neither random with age nor does it display cyclicity, and because our trend of data from U1337 fits better, after extrapolation, with the biostratigraphic ages for U1338 than with the astrochronometric ages. For compilations, see Westerhold et al. (2020), Holbourn et al. (2022, 2024) and Hilgen (2025).

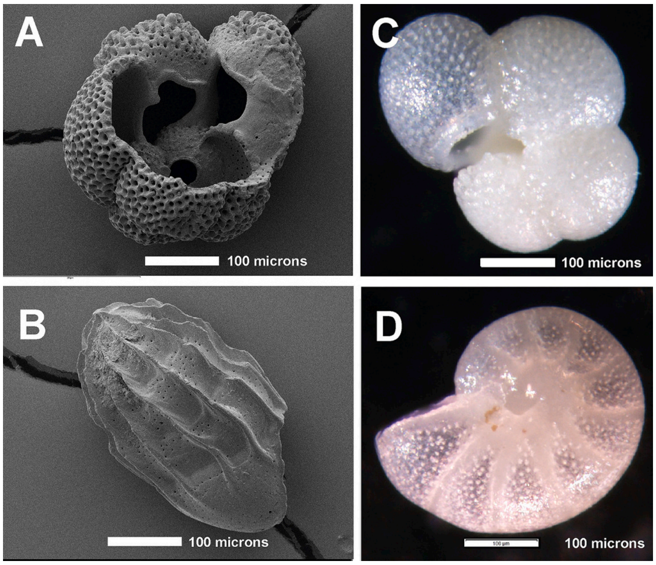

Fig. 3. Examples of cleaned planktic and benthic foraminifera analysed in this study. A. SEM of a broken planktic foraminifera showing empty chambers, unfilled pores, and little overgrowth (1146C 48X-3-W, 134-136). B. SEM of benthic foraminifera showing little overgrowth and open pores (1146C 48X-3-W, 134-136). C. Reflected-light image of a planktic foraminifera showing an empty, glassy, final chamber and semi-glassy earlier chambers and little overgrowth (1146A-49X-4-W, 79-81). D. Reflected light image of a benthic foraminifera showing no overgrowth, glassy calcite, empty chambers and nannofossil-filled (?) pores (U1338B-41H-1-W, 22-23).

2.2. Sample Preparation and preservation

Plugs of 20 g were washed of fines to isolate the fraction >250 μm, which comprised mostly foraminifera but with common echinoid spines and rare ostracod shells. That fraction was then repeatedly washed under ultrasonic agitation in alternating ultra-pure water and ultra-pure water/methanol mixes, for three to five minutes each time, until the supernatant was judged to be free of fines. From each washed fraction, 50 to 100 of the best-preserved microfossils were picked under the microscope for analysis. Samples from two levels in U1337 contained no carbonate microfossils >63 μm: A-36X-4-W, 112-114 and C-22X-2-W, 123-125.

In washed samples prior to picking, microfossils showed a range of preservation from frosty with overgrowths (mostly planktic foraminifera) to glassy without overgrowths (mostly benthic foraminifera and echinoid spines). Picked specimens had open pores, little or (for most) no overgrowths, and no infillings (Fig. 3). For Sites 1264, U1137, and U1338, picked microfossils were overwhelmingly benthic foraminifera and echinoid spines that were glassy or semi-glassy, with <5 % slightly opaque (slightly frosty) planktic specimens. For Site 1146, benthic foramaminifera were similarly well-preserved but were sparse and so supplemented by ≈ 30 % of planktic foraminifera that were semi-glassy or slightly frosty. For two levels in 1146A (48X-5-W, 12-14 cm, 49X–5-W, 145-147 cm), no good material was available so picked samples were > 85 % frosty planktic foraminifera. Our view of preservation agrees with that of Fox et al. (2021) who assessed foraminiferal preservation at Sites 1146 as good to very good, and better at Site U1338 (*ibid.*, Fox and Wade, 2013). From the above, samples were judged to have preserved their original $^{87}Sr/^{86}Sr$ values baring the two exceptions note above.

2.3. Analysis for $^{87}Sr/^{86}Sr$

Chemical preparation and mass-spectrometric analysis was done at the National Environmental Isotope Facility (NEIF) at BGS, Keyworth, UK. Samples were pre-leached by immersion in 1 ml of ultrapure water to which was added 10 μl of Romil® UpA acetic acid. The reaction was allowed to go to completion and then the supernatant was discarded. The remaining sample was dissolved in Romil® UpA acetic acid, the supernatant separated and evaporated to dryness with nitric acid to convert to the nitrate salt, and Sr was separated by ion-exchange chromatography using Sr-spec® resin.

Acquisition of $^{87}Sr/^{86}Sr$ was *via* a Triton mass spectrometer run with the "Sr Triple" multi-dynamic peak-switching routine, with amplifier rotation, and acquisition of between 300 and 600 ratios per sample/standard at 8 to 10 V for ^{88}Sr on resistors of 10^{11} Ω. Integrations times were 8 s for each step of the routine, with 3 s allowed for magnet settling, giving a typical run time of four to five hours. Values of $^{87}Sr/^{86}Sr$ were corrected for isotopic fractionation by adjustment to $^{86}Sr/^{88}Sr$ of 0.1194 using an exponential correction (Thirlwall, 1991). Blanks at NEIF for Sr are routinely < a few tens of picogrammes and so insignificant given our sample masses of 3–5 μg of Sr.

Isotopic analysis was done during three periods: Period 1 was between May and September 2023; Period 2 was between February and May 2024; Period 3 was between December 2024 and February 2025. In Period 1, samples were run on single Re filaments with TaO as activator. In Periods 2 and 3, in order to reduce fractionation, samples were loaded in dilute HNO_3/H_3PO_4 on double Re filaments. Between Period 1 and 2 the electronics of the mass spectrometer were recalibrated using the Thermo Matrix Calibration script. The recalibration decreased all standards values by 0.000 006 6 and so, presumably, also decreased all measured sample values.

2.4. Standards

During this work, we analysed 5 standard materials (NIST987, E&A, EN-1, N-1 and N-2) a total of 125 times in order to quantify the differences between them of the values of $^{87}Sr/^{86}Sr$. The standard SRM987 (also known as NIST987) is a $SrCO_3$ distributed by the National Institute of Standards and Technology, U.S. Department of Commerce. EN-1 is the powdered shell of a modern *Tridachna* clam from Eniwetok Atoll (Ludwig et al., 1988): once distributed by the United States Geological Survey; it appears no longer to be commercially available (USGS, 2024). The standard E&A is a $SrCO_3$ from the Eimer and Amend Company of New York (later acquired by the Fisher Chemical); it also appears no longer to be commercially available. The standard N-1 is a modern nautilus from the collections of University College London and N-2 is a modern nautilus obtained as bycatch by a fishery in Queensland, Australia. To supplement our own standards analysis, we compiled data from the literature (legacy data) in which two or more of the common standards NIST(SRM)987, EN-I and E&A were reported as analysed in the same session.

To further clarify the best value of $^{87}Sr/^{86}Sr$ in SRM987 to use for normalisation, we downloaded and processed data for SRM987 from the GeoRem database (Jochum et al., 2007) and refined the data as follows. By reference to original publications, we removed entries that reported erroneous data (overwhelmingly error in the original publication rather than error in data entry into GeoRem *e.g.* a value of 0.701 234 for SRM987 reported in a publication and so entered into GeoRem was removed rather than corrected to 0.710 234). Thereafter, data were included only if acquired after 1999 by TIMS. Duplicate entries were removed and data were rejected where 2 s.d. / 2 s.e. were greater than 0.000 020 / 0.000 010. Data given to 5 d.p. were then checked in the original publication and truncation/addition of trailing zeros was corrected *e.g.* where an entry read 0.710 21 in the database but 0.710 210 in the original paper and *vice versa*. From the pool of surviving data, we then extracted for use only that data that had 6 d.p. and fell within 3 s.d. of the mean of the pool. Surviving data numbered 949 out of 2389 (as of 20 10 2024).

In order to examine long-term trends in measured values for SRM987, we compiled $^{87}Sr/^{86}Sr$ acquired with the Triton at NEIF over a 9-year period. Finally, to assess the sensitivity, if any, of our measured

Table 1
Measured and normalised values of $^{87}Sr/^{86}Sr$ for standards analysed during the three periods during which analysis for this work was done. Where normalised, it is to the $^{87}Sr/^{86}Sr$ value of 0.710 248 for SRM987. MSS is modern-marine Sr, a grand mean of values for EN-1, N1, and N2. Period 1, May to September, 2023; Period 2, February to May, 2024; Period 3, December, 2024 to January, 2025.

Period	Standard	Measured $^{87}Sr/^{86}Sr$	2 s.e. $\times 10^{-6}$	*n*	Normalised $^{87}Sr/^{86}Sr$
1	SRM987	0.710 262	0.9	26	0.710 248
2	SRM987	0.710 255	1.5	18	0.710 248
3	SRM987	0.710 258	1.9	9	0.710 248
1	MSS (EN-1, Ni, N2)	0.709 186	1	15	0.709 171 4
2	MSS (EN-1, Ni, N2)	0.709 180	1.1	27	0.709 172 9
3	MSS (EN-1, Ni, N2)	0.709 182	2.1	9	0.709 171 5
Mean					**0.709 171 9**
2 s.d. of mean					**1.6**
1	E&A	0.708 035	1.3	10	0.708 020 2
2	E&A	0.708 029	1.1	7	0.708 021 5
3	E&A	0.708 032	1.3	4	0.708 021 1
Mean					**0.708 020 9**
2 s.d. of mean					**1.4**
1	(SRM987)-(MSS)	0.001 077			
2	(SRM987)-(MSS)	0.001 075			
3	(SRM987)-(MSS)	0.001 077			
Mean difference		**0.001 076**	**0.9**		
1	(SRM987)-(E&A)	0.002 228			
2	(SRM987)-(E&A)	0.002 227			
3	(SRM987)-(E&A)	0.002 227			
Mean difference		**0.002 227**	**0.8**		

$^{87}Sr/^{86}Sr$ to the intensity of the ion-beam current (here expressed as voltage) we acquired values of $^{87}Sr/^{86}Sr$ measured at NEIF on SRM987 at voltages from 2 to 10 V and from Ando et al. (2010), also with a Triton, on voltages from 5 to 20 V.

3. Results

3.1. Standards data

For our measured $^{87}Sr/^{86}Sr$ for standards, mean values for each period of analysis are given in Table 1. The means for SRM987 during the three analytical periods are 0.710 262 4 ± 0.000 000 9 (2 s.e., n = 26), 0.710 255 2 ± 0.000 001 5 (2 s.e., n = 18), and 0.710 258 4 ± 0.000 001 9 (2 s.e., n = 9). The difference between mean values of SRM987 and MSS (EN-1, N1, N2) is 1076.1 ± 0.9 ($\times 10^6$). The difference between mean values of SRM987 and E&A is 2227.1 ± 0.8 ($\times 10^6$).

To enable further definition of the differences in $^{87}Sr/^{86}Sr$ between standards, Table 2 gives the values, and differences between them, of $^{87}Sr/^{86}Sr$ from the literature for pairs of standards that were each run during a single period of analysis. Excluding outliers shown in italics, the mean value for SRM987 in Table 2 is 0.710 249 8 ± 0.000 001 7 (2 s.e., n = 39). Values of $^{87}Sr/^{86}Sr$ in SRM987 (TIMS data) from the GeoRem database are summarised as a histogram in Fig. 4; the mode of the distribution is 0.710 250 and the mean is 0.710 249 0 ± 0.000 001 0 (2 s.e., n = 949).

Uncertainties associated with mass-spectrometry are illustrated in Fig. 5, which shows, for seven separate mass-spectrometric runs of SRM987, how 2 s.d., 2 s.e. and exponentially-corrected (final) $^{87}Sr/^{86}Sr$ change as a function of the number of ratios measured. Beyond accumulation of 250 ratios, little improvement occurs to the standard deviation of the data (Fig. 5A) although standard error (s.d./$n^{½}$) continues to decline (Fig. 5B) because n, the number of ratios accumulated, continues to increase. Accumulation of more than 250 ratios does not change the mean value of $^{87}Sr/^{86}Sr$ by more than 0.000 001 (Fig. 5C).

How the strength of the ion-beam current affects measured $^{87}Sr/^{86}Sr$ is shown in Fig. 6. For the Triton in static mode (Ando et al., 2010), the effect on $^{87}Sr/^{86}Sr$ of differing measured voltages (ion-bean currents) is no more than 0.000 000 41 per volt (Fig. 6A), whereas the effect on the NEIF Triton in dynamic mode appears to be zero (Fig. 6B).

On a longer time-scale, Fig. 7 shows a plot of turret means for SRM over a nine-year period for in which two or more measured $^{87}Sr/^{86}Sr$ for SRM987 were obtained (*cf.* Figs. A1–4 of Andrews et al., 2016). Turret means range from 0.710 244 to 0.710 266. The mean value is 0.710 253 4 ± 0.000 008 4; 2 sd, n = 215). A linear regression to the data rises only by 0.000 000 2 over the nine years, but values drift downwards through 2011 to a minimum in late 2012 before recovering to previous values by early 2014: at ***a***, 24 consecutive turrets are stable with a mean of 0.710 252 8 (2 s.d. = 0.000 004 0). At ***b***, three consecutive turrets have low values ≈ 0.710 246. At ***c***, turret means are 0.000 008 below the long-term mean and at ***d*** they are 0.000 009 above it.

3.2. Sample data

Values of $^{87}Sr/^{86}Sr$ referred to in the text, plotted in figures, and used for regression analysis, are normalised periodwise to a value of 0.710 248 0 for each of our three periods of analysis. Measured and normalised values of $^{87}Sr/^{86}Sr$ in samples are given in Table 3 and the latter are shown graphically in Figs. 8 and 10. Also on Fig. 8 is plotted for reference the $^{87}Sr/^{86}Sr$-reference line of McArthur et al. (2020; LOWESS 7).

A plot of all data to the CENOGRID ages (1146, 1264, U1337) and bio-magnetostratigraphic ages (U1338) is shown in Fig. 8A. The new data plot below the LOWESS 7 line at ages >15 Ma and above it at younger ages. Four portions of the plot in Fig. 8A show anomalies at B, C, D and E, and these are shown in more detail in Fig. 8B, C, D, and E, and are discussed below.

Between 12.7 and 15.5 Ma, data for U1338 form a well-defined curve (Fig. 8B), but four values of $^{87}Sr/^{86}Sr$ at ≈ 14 Ma plot off the regression fit to the other data. The aberrant samples are from Core 38 of Hole C and Core 38 of Hole B. One of these samples, U1338C-38H-1-W, 122-124 has an unusually large uncertainty of ±0.000 008 and so is within uncertainty of the trend.

Values of $^{87}Sr/^{86}Sr$ for Sites 1146 and U1338 are discordant (Fig. 8C). At ages <12.2 Ma, data for 1146A and 1146C are concordant; at older ages, 1146C plots ≈ 0.2 myrs older than 1146A. Although on Fig. 8C samples from U1338C plot below those from U1338B, the separation is not greater than analytical uncertainty and is not seen across the total age-range for U1338 samples (Fig. 8B), so we treat ages of samples from U1338B and U1338C as concordant.

Of our $^{87}Sr/^{86}Sr$ plotted in Fig. 8D, a single regression line (green line) encompasses five of the eight samples from Site 1264, plotted against CENOGRID ages, all nine samples from U1337 for which Hilgen (2025) ages are available (Table 3) and the four of the five youngest samples from U1337 plotted against CENOGRID ages (which are indistinguishable from Hilgen ages at <16.5 Ma). The regression line is parallel to the LOWESS regression line, shown in blue. The green regression line in Fig. 8D,E is a second-order fit with a Pearson ***r*** of 0.999 721:

$$\text{Age} = -416{,}437.3460044860 * R^2 + 576{,}816.21788458 * R - 199{,}615.235613129,$$

where $R = {}^{87}Sr/^{86}Sr$

A linear fit is all but identical (Pearson ***r*** of 0.999 716). The regression line was used to derive $^{87}Sr/^{86}Sr$-ages for samples from U1337 and 1264 that are off the regression line when plotted to CENOGRID ages, *i.e.* samples with apparently aberrant ages (Fig. 8D,E). These $^{87}Sr/^{86}Sr$-ages are given in Table 3. Use of a linear regression resulted in ages that differed by no more than 9 kyrs from those derived from the second-order regression. We prefer the second-order regression as the LOWESS reference curve has slight curvature towards the top end of the age range seen in samples from U1337 and because it provides an almost perfect match to data from U1338 (Fig. 8F).

As Fig. 8D shows, the trend of data for U1337 plotted to CENOGRID ages differs by up to 400 kyrs from the trend of data defined by the green regression line. The trends are concordant at ages <16.5 Ma and approach concordance at 20 Ma, but depart from each other by up to

Table 2

Literature values of $^{87}Sr/^{86}Sr$ for standards SRM987, and EN-1 or its equivalent, that were run in the same analytical period. Empty cells denote a lack of data. Cells shaded in light blue are normalised to an author's value for their chosen standard, as un-normalised data were not reported. Data in italics are considered outliers. Data for Periods 2 and 3 of this work are not included in the statistical calculations. in order to avoid over-biasing the result. The references cited in the table are listed in the Supplementary Information.

Standard	Meaqsured E&A	2.s.e $x10^6$	n	Measured SRM987	2.s.e $x10^6$	n	Δ $x10^6$	2.s.e $x10^6$	Year	Value to 248	Author	Machine type	Laboratory	Comment
E&A	0.708066	5.3	24	0.710275	5.3	24	2209		1985	0.708039	Palmer and Elderfield 1985	VG Micromass	Leed University	St devs. not given, so sd is for modern forams
E&A	0.708000			0.710220			2220		1986	0.708028	Hess et al. 1986			
E&A	0.708028	0.9	34	0.710254	1.2	26	2226	1.5	1994	0.708022	Jones et al. 1994	VG Isomas 54E	U. Oxford	
E&A	0.708027	13	2	0.710248	13	5	2221	18	2000	0.708027	Hesselbo et al. 2000	VG Isomas 54E	U. Oxford	
E&A	*0.707988*	*18*		*0.710179*	*13*	*4*	*2191*		2006	0.708057	Park et al. 2006	MAT 262	U. Melbourne	*n* . not given for E&A
E&A	0.708059	33	5	0.710261	5	33	2202	33	2013	0.708046	Beard et al. 2013	VG Sector 53	Not specified	Small Sr-loads
E&A	0.708012	5	10	0.710239	3	20	2227	6	2016	0.708021	du Bray et al. 2016	Triton Ti	Carlton University	
E&A	0.708055	8	8	0.710270	3	35	2215	9	2017	0.708033	Satkoski et al. 2017	VG Sector 54	University of WisconsinMadison	
E&A	0.708035	1.3	10	0.710262	0.9	26	2228	1.6	2024	0.708020	This work, Period 1	Triton	NEIF, Keyworth, UK	
E&A	0.708029	3	7	0.710255	1.5	18	2227	3.4	2024	0.708022	This work, Period 2	Triton	NEIF, Keyworth, UK	
E&A	0.708032	1.3	4	0.710258	1.9	9	2227	2.3	2024-5	0.708021	This work, Period 3	Triton	NEIF, Keyworth, UK	
Mean							**2214**			**0.708034**				
2.s.d.							**29**			**0.000029**				
n							**6**			**6**				
2 s.e.							**12**			**0.000012**				
SW (CIT Standard)	*0.709242*	25		*0.710310*	5.0		1068		1983	0.709180	DePaolo et al 1983		University of California?	Uncertainty = 2 s.d. *n* not given
Modern shells	*0.709234*	4.2	18	*0.710330*	3.2	10	1096	5	1985	0.709152	DePaolo and Ingram 1985		University of California	Some data retrospective from Richter & DePaolo 1988
Modern foraminifera	0.709244	5.3	24	0.710275	5.3	24	1031	8	1985	0.709217	Palmer and Elderfield 1985	VG Micromass	Leeds University	SW from modern forams in Palmer 1983; s.d from P&E 1985
Foraminifera	0.709174	8.4	11	0.710235	2.9	58	1061	9	1990	0.709187	Hodell et al. 1990	VG 354	U Florida	Samples < 15ka, KNR31-GPC5
Foraminifera	0.709174	9.3	11	0.710235	2.9	58	1061	10	1990	0.709187	Hodell et al. 1990	VG 354	U Florida	Samples < 32 ka, EN32-PC6
EN-1	0.709172			0.710235	2.9	58	1063		1990	0.709185	Hodell et al. 1990	VG 354	U Florida	Normalisation suspect
SW (National Inst Oceanog.)	0.709166	6.7	5	0.710241	22		1075		1990	0.709173	McArthur et al. 1990	VG354	RHBNC	Uncertainty for SRM987 = 2 s.d.; *n* not given
EN-1	0.709197	7.0	22	0.710245	4.0	55	1048	8	1991	0.709200	Carpenter et al. 1991	VG Sector	Univ. Michigan?	Uncertainty quoted as 2σ are probably 2 s.e.
SW (Atlantic)	0.709171	6.5	6	0.710231	3.1	20	1060	7	1991	0.709188	Brand 1991	Finnigan-MAT 262	Ruhr-Universität Bochum	
SW	0.709191	18	2	0.710252	4.4	35	1061	19	1991	0.709187	Miller et al. 1991	VG Sector 54	Rutgers Univ.	SW mean of two, *pers. com* Miller 1992; se from SRM987
SW	0.709174	5.0		0.710241	8.0		1067	9	1991	0.709181	Asmerom et al. 1991	Finnigan-MAT 262		Uncertainty probably = 2 s.e, but *n* is not known..
EN-1	0.709178	0.6	27	0.710245	0.2	77	1067	0.6	1991	0.709181	Quinn et al. 1991	VG Sector	U. Michigan?	
SW (N. Atlantic, C Pacific)	0.709175	22		0.710265	22		1090		1991	0.709158	Martin and MacDougall 1991			Uncertainty probably = 2 s.d.
Seawater	*0.70916*	20		*0.710233*	20		1073		1991	0.709175	Podosek et al. 1991	VG354	Washington Univ, St Louis	Uncertainty at 2 s.d., n not specified
SW (North Sea)	0.709168	29	1	0.710234	23	1	1066	37	1992	0.709182	Andersson et al. 1992	Lunatic 1	Cal. Inst. Technology	
SW	0.709174	5.0		0.710241	8.0		1067		1992	0.709181	Derry et al. 1992	Finnigan-MAT 262	Harvard University ?	Uncertainty = 2 s.d.
SW, N-1 (modern nautilus)	0.709175	12		0.710248	18		1073		1992	0.709175	McArthur et al. 1992	VG 354	RHBNC	Uncertainty = 2 s.d.
Modern shells	0.709167	2.3	33	0.710244	2.0	48	1077	3	1992	0.709171	Dia et al. 1992	VG 354	Cambridge University	Intercept t = 0, of linear fit to all data *v* age
Modern coral	0.709154	3.5	16	0.710232	6.4	18	1078	7	1992	0.709170	Ohde and Elderfield 1992	VG 54E	Univ. Cambridge	
SW (CIT)	0.709150	24	1	0.710234	23	1	1084	33	1992	0.709164	Andersson et al. 1992	Lunatic 1	Cal. Inst. Technology	Uncertainty = 2 s.d.
EN-1	0.709175	2.0	75	0.710262	2.2	103	1087	3	1992	0.709161	Sinnesael et al. 2019 (1992)	VG 354	UC Berkely	1992 data. Table DR3. Long-term average implied
SW (Pacific Ocean)	0.709174	5.0		0.710241	8.0		1067		1993	0.709181	Kaufman et al. 1993	Finnigan-MAT 262	Harvard University ?	Uncertainty = 2 s.d.; *n* not given
SW (NASS-2)	0.709175	24		0.710260	24		1085		1993	0.709163	Paytan et al. 1993		Scripps Inst. Ocean.	Uncertainty for SRM987 = 2 s.d.
Modern SW	0.709170	4.6	16	0.710260	24		1090		1993	0.709158	Paytan et al. 1993		Scripps Inst. Ocean.	Uncertainty for SRM987 = 2 s.d.
EN-1	0.709191	5.0	2	0.710255	3.6	20	1064	6	1994	0.709184	Oslick et al. 1994	VG Sector 54	Rutgers University	Uncertainty for EN-1 = deviation from mean
Foaminifera	0.709159	1.0	48	0.710233	9.0	82	1074	9	1994	0.709174	Henderson et al. 1994	VG 354	U. Cambridge	Intercept t = 0, of linear fit to all data *v* age
EN1	0.709166	8.9	5	0.710231	6.8	17	1065	11	1997	0.709183	Winter et al. 1997	VG Sector 54	University of Wisconsin	
SW, Arctic Ocean	0.709186	2.1	16	0.710264	0.9	18	1078	2	1997	0.709170	Winter et al. 1997	VG Sector 54	University of Wisconsin	
EN1	0.709185	4.5	7	0.710264	0.9	18	1079	5	1997	0.709169	Winter et al. 1997	VG Sector 54	University of Wisconsin	
EN1	*0.709254*	2.4	24	*0.710338*	5.3	17	1084	6	1997	0.709164	Winter et al. 1997	VG Sector 54	University of Wisconsin	
EN-1	0.709176	21.0	2	0.710248	12.5	5	1072	24	2000	0.709176	Hesselbo et al. 2000.	VG54E	University of Oxford	
EN-1	0.709175	3.2	19	0.710248	2.5	19	1073	4	2000	0.709175	McArthur et al. 2000.	VG354	RHUL	
SW (Meditteranean)	0.709175			0.710232	3.0	45	1057	3	2003	0.709191	Sprovieri et al. 2003	Finnigan-MAT 262 RPQ	C.N.R., Rome	
SW (off Norway & France)	0.709149	4.5	20	0.710238	2.9	6	1089	5	2003	0.709159	Brand et al. 2003	Finnigan-MAT 262	Ruhr-Universität Bochum	
Modern shells	0.709148	4.0	30	0.710238	2.9	6	1090	5	2003	0.709158	Brand et al. 2003	Finnigan-MAT 262	Ruhr-Universität Bochum	

EN-1	0.709173	1.6	10	0.710248			1075		2006	0.709173	McArthur et al. 2006	VG354	RHUL	
SW (source unspecified)	0.709175			0.710241	11		1066		2006	0.709182	Fantle and DePaolo 2006	Triton	UC Berkeley	2 s.d. assumed for SRM987; no sd given for SW
EN-1	0.709156	4.5	4	0.710238	8.0	4	1082	9	2007	0.709166	Buhl et al. 2007	Finnigan-MAT 262	Ruhr-Universität Bochum	
EN-1	0.709191	14	3	0.710255	2.4	11	1064	15	2008	0.709184	Melezhik et al. 2008	Triton	IPGG, RAS, St Petersburg	
EN-1	0.709180	3.3	11	0.710253	2.9	73	1073	4	2009	0.709175	Miller et al. 2009	FinniganMAT-261	U. Texas, Dallas	Static measurements, assume 2.sd for calculation.
Recent Foraminifera	0.709176	2	14	0.710248	1.6	20	1072		2010	0.709176	Ando et.al. 2010	Triton	RIHN, Kyoto	Foraminifera < 30 Ka
Recent Corals	0.709174	1.5	27	0.710248	1.3	14	1074		2010	0.709174	Ando et al. 2010	Triton	RIHN, Kyoto	Corals < 10 Ka
SW (Pacific)	0.709173	2.7	5	0.710248	1.3	14	1075		2010	0.709173	Ando et.al. 2010	Triton	RIHN, Kyoto	
EN-1	0.709157	2.2	157	0.710239	2.9	169	1082	4	2010	0.709166	Brand et al. 2010	Finnigan-MAT 262	Ruhr-Universität Bochum	May be 1 s.e.
EN-1	0.709176	1.4	561	0.710249	1.3	442	1073	2	2011	0.709175	Uysal et al. 2011	VG Sector 54	University of Queensland	6-year means
EN-1	0.709159	2.1	182	0.710240	2.6	193	1081	3		0.709167	Brand et al. 2012	Finnigan-MAT 262	Ruhr-Universität Bochum	
EN-1 (2009/10)	0.709202	1.2	26	0.710275	1.1	54	1073	2	2012	0.709175	Kuznetsov et al. 2012	Triton	GI/IGM, RAS	
Modern shells ((2009/10)	0.709202	1.3	33	0.710275	1.1	54	1073	2	2012	0.709175	Kuznetsov et al. 2012	Triton	GI/IGM, RAS	Modern shells, Atlantic, Pacific, Indian, coasts
SW (source unspecified)	0.709169	3.5	23	0.710243	2.5	45	1074	4	2012	0.709174	Chapman et al. 2012.	Finnigan-MAT 262	University of Pittsburg	s.d. for SW not given, so set equal to s.d. for SRM987
EN-1	0.709180	7.2	28	0.710252	3.8	40	1072	8	2012	0.709176	Williamson et al. 2012	VG54-30		Static measurements
EN-1	*0.709177*	0.3	77	*0.710280*	1.6	19	*1103*	2	2012	*0.709145*	Peterman et al. 2012	Finnigan-MAT 262	USGS, Denver?	
Modern shells	0.709165	2.1	13	0.710240			1075		2014	0.709173	Vollstaedt et al. 2014	Triton	GEOMAR, Kiel	No uncertainty for SRM987
SW (NASS-6)	0.709179	1.8	8	0.710248			1069		2014	0.709179	Neymark et al. 2014	Triton	USGS, Denver	Table 2. normalised, so no uncertainty for SRM987
EN-1	0.709176	3.0	28	0.710248			1072		2014	0.709176	Neymark et al. 2014	Triton	USGS, Denver	Table 2. normalised, so no uncertainty for SRM987
Acan-1 (acantharia)	0.709173	5.0	8	0.710248			1075		2014	0.709173	Neymark et al. 2014	Triton	USGS, Denver	Table 2. No uncertainty for SRM987. Acantharia are $SrSO_4$
Seawater (Atlantic Ocean)	0.709178	1.3	10	0.710256	0.7	23	1078	2	2015	0.709170	Mokadem et al. 2015	Triton	Durham University	
EN-1	0.709178	3.5	2	0.710256	1.2	18	1078	4	2015	0.709170	Melezhik et al. 2015	Triton TI	IPGG, RAS, St Petersburg	
JCp-1	0.709168	6.0	10	0.710246	5.5	16	1078	8	2015	0.709170	Voigt et al. 2015	Triton	GEOMAR, Kiel	
SW (IAPSO)	0.709167	1.8	5	0.710246	5.5	16	1079	6	2015	0.709169	Voigt et al. 2015	Triton	GEOMAR, Kiel	
EN-1	0.709194	10	12	0.710262	2.0	66	1068	10	2017	0.709180	Baddouh et al. 2017	VG 354	University of Wisconsin-Madison	
EN-1	0.709194	4.6	8	0.710270	2.7	35	1076	5	2017	0.709172	Satkoski et al. 2017	VG Sector 54	University of WisconsinMadison	
EN-1	0.709160	1.4	209	0.710240	2.2	233	1080	3	2017	0.709168	Fichtner et al. 2017	Finnigan-MAT 262	Ruhr-Universität Bochum	Whether 1 sd or 2 sd not specified; assumed 2 sd
EN-1	0.709197	3.0	11	0.710256	2.1	19	1059	4	2017	0.709189	Kuznetsov et al. 2017	Not clear		Mat 262 or Triton - which is not clear.
EN-1	0.709163	2.2	26	0.710240	1.4	>100	1077	3	2017	0.709171	Dudás et al. 2017	TIMS (make not given)	Mass. Inst. Technol. ?	2.s.e. calculated on n = 100
EN-1	*0.709214*	1.5	16	*0.710285*	2.0	16	*1071*	3	2018	*0.709177*	Dipre et al. 2018	Triton	IPGG, RAS	
SW (coastal Australia)	0.709168	1.6	24	0.710248			1080		2018	0.709168	Farkaš et al. 2018	VG Sector 54 IT	Univ. Copenhagen	No uncertainty for SRM987
SW (coastal Australia)	0.709166	1.6	10	0.710248			1082		2018	0.709166	Farkaš et al. 2018	VG Sector 54 IT	Univ. Copenhagen	No uncertainty for SRM987
Modern shells	0.709176	7.0	31	0.710245	5.5	12	1069	9	2018	0.709179	El Meknassi et al. 2018	Triton Plus / MAT 261	GET, Toulouse	Shells, unrestricted Atlantic and Pacific coasts; 31 samples .
Core top	0.709179	1.7	4	0.710252	3.1	13	1073	4	2019	0.709175	Matsui et al. 2019	VG Sector 54-30	Nagoya University	Intercept t = 0, of linear fit to 4 samples <0.8 Ma
EN-1	0.709153	3.9	24	0.710240	3.9	34	1087	6	2019	0.709161	Zaky et al. 2019	TiBox Spectromat	Ruhr-Universität Bochum	Average for the paper's period of study
EN-1	0.709171	12	6	0.710253	3.1	50	1082	12	2020	0.709166	Nádaskay et al. 2020	Triton Plus	Czech Geological Survey, Prague?	
EN-1	0.709173	0.6	175	0.710251	0.4	263	1078	1	2021	0.709170	Paces et al. 2023	Triton	USGS Denver	Five-year average values
EN-1	0.709171	9.0	6	0.710252	2.1	109	1081	9	2022	0.709167	Erban-Kochigina 2022	Triton Plus	Czech Geological Survey	
EN-1	0.709163	37		0.710246	27		1083		2022	0.709165	Bosio et al. 2022	TI-Box Spectromat	Ruhr-Universität Bochum	Uncertainty = 2 s.d. of "long-term" means
Seawater (S. Pacific Ocean)	0.709177	2.7	6	0.710251	0.6	43	1074	3	2021	0.709174	Di et al. 2021	Triton	ANU, Canberra	
EN-1	0.709156	6.8	22	0.710240	3.0	22	1084	7	2021	0.709164	Wang et al. 2021	TiBox Spectromat	Ruhr-Universität Bochum	
EN-1	0.709170			0.710246			1076		2023	0.709172	Coimbra et al. 2023	Finnigan-MAT 262	Ruhr-Universitlt Bochum	No uncertainties given. Long-term means
EN-1	0.709175	2.3	3	0.710250	0.5	14	1075	2	2024	0.709173	Zakharov et al. 2024	Triton TI	IPGG, RAS, St Petersburg	
Holocene coral	0.709166	1.7	13	0.710242	1.0	39	1076	2	2024	0.709172	Wang et al. 2024	Phoenix	Stony Brook University, New York	
EN-1	*0.709206*	1.6	18	*0.710277*	0.8	25	*1071*	2	2024	*0.709177*	Efremenko et al. 2004	Triton	IPGG, RAS, St Petersburg	
EN-1, N1, N2.	0.709186	1.0	15	0.710262	0.9	26	1076	1	2024	0.709172	This work (Period 1)	Triton	NEIF, Keyworth, UK	N1, N2, are separate specimens of modern nautilus.
EN-1, N1, N2.	0.709180	1.1	27	0.710255	1.5	18	1075	2	2024	0.709173	This work (Period 2)	Triton	NEIF, Keyworth, UK	N1, N2, are separate specimens of modern nautilus.
EN-1, N1, N2.	0.709182	2.1	9	0.710258	1.9	9	1076	3	2024-5	0.709172	This work (Period 3)	Triton	NEIF, Keyworth, UK	N1, N2, are separate specimens of modern nautilus.
EN-1	0.709140	15		0.710230	40		1090		2014	0.709158	Brenna 2014	Nu Plasma ICP-MC-MS	University of Melbourne	Uncertainty at 2.s.d; *n* not given
EN-1	0.709155	5.4	47	0.710230	30		1075		2017	0.709173	Belli et al. 2017	Nu Plasma ICP-MC-MS		Uncertainty for SRM987 at 2.s.d.
JCp-1	0.709170	6.0	3	0.710248	4.3	14	1078	7	2017	0.709170	Weber et al. 2017	Neptune ICP-MC-MS	CIGS, Univ. Modena	
JCt-1	0.709169	9.0	3	0.710248	4.3	14	1079	10	2017	0.709169	Weber et al. 2017	Neptune ICP-MC-MS	CIGS, Univ. Modena	
EN-1	0.709156	2.7	35	0.710230			1074		2017	0.709174	Ribeiro et al. 2017	Nu Plasma ICP-MC-MS	Univ. Melbourne	No data for uncertainty on SRM987
SW (IAPSO)	0.709169			0.710247	2.4	63	1078		2020	0.709170	Scaffidi et al. 2020	Neptune ICP-MC-MS	Arizona State University	No uncertainty given for SW
SW (IAPSO)	0.709175	3.0	55	0.710249	2.9	75	1074	4	2023	0.709174	Avigliano et al. 2023	Neptune Plus	Inst. Earth Sci., Acad. Sinica, Taiwan	Long-term means
SW (IAPSO)	0.709175	2.0	35	0.710250	0.9	125	1075	2	2023	0.709173	Wang et al. 2023	Neptune ICP-MC-MS	Yale	Wang et al's 2σ is actually 2 se
SW (IAPSO)	0.709156	3.8	89	0.710247	1.0	490	1091	4	2023	0.709157	Choi et al. 2023	Neptune ICP-MC-MS	Korea Basic Science Inst., Chungbuk	
	Without normalised standards						**With normalised standards**				RAS = Russian Academy of Sciences. RHBNC = Royal Holloway and Bedford New College (now Royal Holloway, University of London, RHUL)			
Mean post 1999, by TIMS	**0.7091741**			**0.7102498**			**1075.5**			**0.7091725**				
2.s.d.	**0.0000146**			**0.0000109**			**13**			**0.0000065**				
n	**39**			**39**			**49**			**49**				
2 s.e.	**2.3**			**1.7**			**1.9**			**0.9**				
Max							**1103**			**0.709217**				
Min							**1031**			**0.709145**				
Range (x $10^{6)}$							**72**			**72**				

RAS = Russian Academy of Sciences. RHBNC = Royal Holloway and Bedford New College (now Royal Holloway, University of London, RHUL).

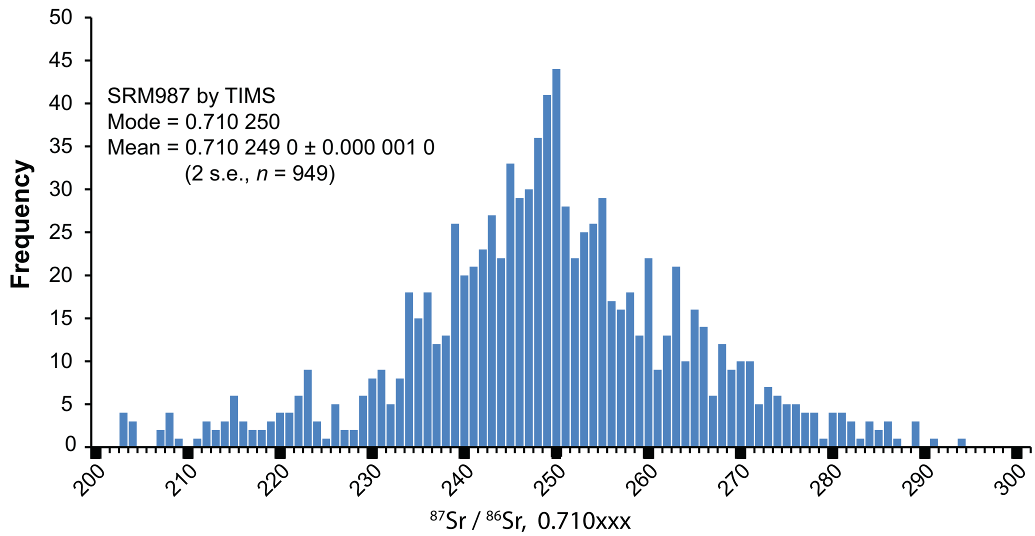

Fig. 4. Histogram of values of $^{87}Sr/^{86}Sr$ for SRM987 measured by TIMS in a subset of data from the GeoRem database (Jochum et al., 2007). See the text for details of how the subset was obtained.

400 kyrs at ages between. Four samples from U1337D-40X are identified by arrows, which all have CENOGRID ages that are 400 kyrs less than predicted by the regression line.

In Fig. 8E, our $^{87}Sr/^{86}Sr$ data for 1264, and data of Stoll et al. (2023) for Site 1218, are compared to the regression line (green line) from Fig. 8D. Three of eight samples from Site 1264 plot off the regression line, so $^{87}Sr/^{86}Sr$ ages were calculated for these three samples (Table 3). Of the four data of Stoll et al. (2023), two plot on the regression line and two plot above it by 0.000 024 and 0.000 014.

Finally, we compare regression lines of $^{87}Sr/^{86}Sr$ *versus* age for U1338 and U1337 in Fig. 8F and in Fig. 10 shows all data plotted to our preferred ages (Table 3) along with, for comparison, previous reference curves for the interval from McArthur et al. (2012, McArthur et al., 2020). The second-derivative of the 5th-order polynomial fit to the data in the age-range 12.7.3 to 17.5 Ma (red hatched line) identifies 15.1 Ma as the point of maximum rate of change, with the decrease in slope starting at 16.0 Ma and ending at 13.6 Ma.

4. Discussion

4.1. Standards

Different laboratories report different values of $^{87}Sr/^{86}Sr$ on analysing the same homogenous material, whether that material is a sample or a standard (Fig. 4, Table 2). To remove this *interlaboratory bias*, all $^{87}Sr/^{86}Sr$ for a study are adjusted (normalised) to an accepted value for a standard by adding or subtracting to each measured value of $^{87}Sr/^{86}Sr$ an amount needed to bring the standard to the accepted value. There are no universally-accepted values for any standard. For SRM987, commonly used values are 0.710 230, 0.710 240, 0.710 248, and 0.710 250. The value of 0.710 248 ± 0.000 000 5 (2 s.e., $n = 427$), given by Thirlwall (1991), is widely used. The mean value of the filtered GeoRem database is 0.710 249. This last value is indicative only because it is a mean that is weighted towards the more active laboratories, the number of entries per laboratory in the GeoRem database ranging widely. The data in Table 2 also gives a mean value of $^{87}Sr/^{86}Sr$ for SRM987 of 0.710 249 but, to avoid such weighting, 5 values reported in the literature were not included in Table 2.

Values of SRM987 from GeoRem and from Table 2 differ by 0.000 001 from the value of Thirlwall (1991), a difference that is within uncertainty limits. We therefore recommend continuing to use the value of 0.710 248 for SIS in order to provide continuity with past usage. On this basis, our value for EN-1 is 0.709 171 9 ± 0.000 001 6 (2 s.e.) and our value for E&A is 0.708 020 9 ± 0.000 001 4 (2 s.e.). For our data, the standard error of the mean (s.e.) is low because we used high beam-currents and accumulated >250 ratios, after which there is little improvement in data quality (Fig. 5). Whilst standard error (s.d./$n^{½}$) continues to decline as the number of ratios collected continues to increase, collection of ≈ 250 ratios may be the best compromise between time spent and uncertainty minimised.

4.2. Residual Bias

Which standard is used for normalising data should not matter because the *difference* between standards should be invariant. Unfortunately, the *difference* between measured values for standards is not the same for all laboratories. For example, in Table 1, the difference between the $^{87}Sr/^{86}Sr$ of SRM987 and EN-1, ($\Delta^{87}Sr/^{86}Sr_{(SRM987\text{-}EN\text{-}1)}$,) is 0.001 076 whilst the difference for other laboratories ranges from 0.001 031 to 0.001 103 (Table 2). This range, of 0.000 072 shows that not all interlaboratory bias is corrected for by normalisation. That part of the bias not corrected we term *residual bias* (McArthur, 1994; Oslick et al., 1994; Martin et al., 1999).

Residual bias may arise from multiple causes (Podosek et al., 1991; Thirlwall, 1991; Di et al., 2021) *e.g.* matrix effects from inefficient purification of Sr prior to analysis by ion-exchange, which SRM987 does not undergo; non-exponential fractionation effects (Di et al., 2021), collector doping and drift (Andrews et al., 2016), undeclared blank problems, operator bias in loading samples onto beads for measurement, baseline settings, magnet- and amplifier-settling times, whether measurements are made in static or dynamic (peak switching) mode (Thirlwall, 1991; Andrews et al., 2016; Schneider and Kleine, 2024), and linearity of amplifier response. On the last, Capo and DePaolo (1990) found that $^{87}Sr/^{86}Sr$ increased by 0.000 010 per volt of $^{88}Sr^{+}$ bean intensity. We found a negligible effect of ion-bean current on $^{87}Sr/^{86}Sr$ (Fig. 6B). Nevertheless, the fact that Martin et al. (1999) ran at 1.5V in dynamic mode on a VG354, Ando et al. (2010, 2011) ran at 20V on a Triton in static mode, and Farrell et al. (1995) ran samples in static mode and standards in dynamic mode, suggests that standardisation of voltage and mode might eliminate potential sources of bias, should they be present.

Our data were obtained during three periods of time. Normalisation of sample data in each period was to standards run in that period. We did not normalise to a long-term mean of standards because instrument response can change with time. Our long-term standards data (Fig. 7) shows sufficient variation to suggest that sample data must be

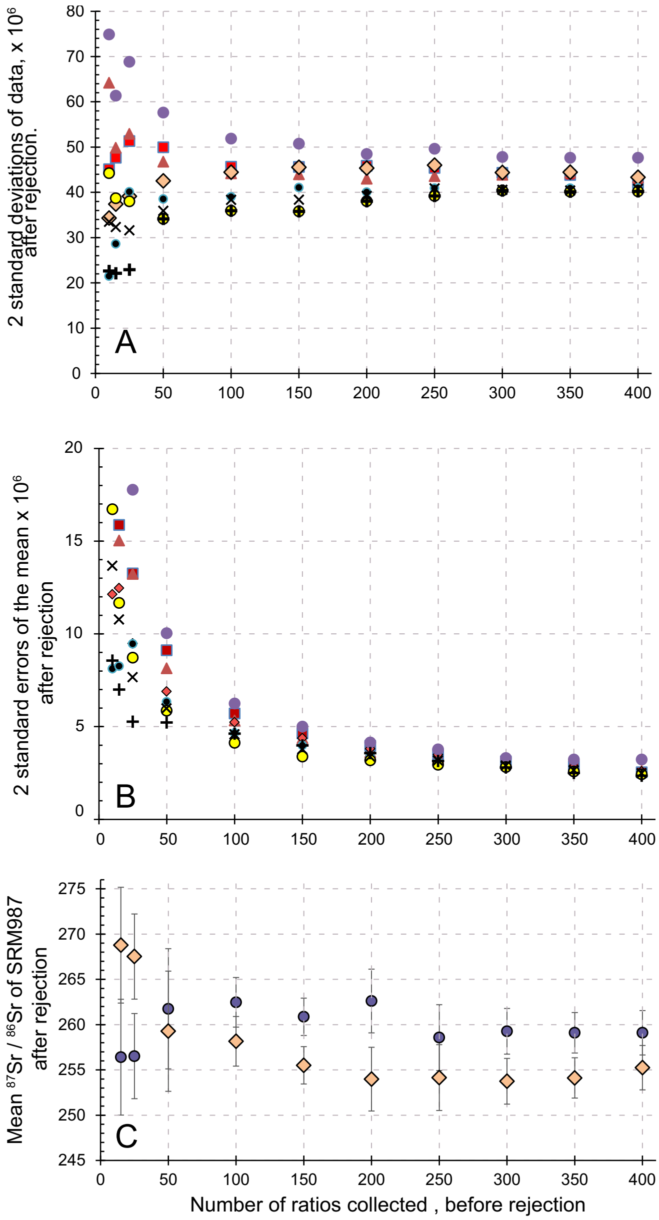

Fig. 5. A. Variation of standard deviation of measurement of $^{87}Sr/^{86}Sr$ (after rejection) with number of ratios, *n*, accumulated (before rejection) during mass spectrometry of 7 standards of SRM987. The different symbols serve only to identify different runs of SRM987. After 250 ratios, little change is seen. B. As A but for standard error of the mean. After 250 ratios, standard error (s.e. = s.d./$n^{1/2}$) continues to decline largely because *n* continues to increase. C. For two standard runs only (for clarity), final values of $^{87}Sr/^{86}Sr$ as a function of *n*; after 250 ratios, change ≤0.000 001.

normalised to standards data that is obtained at the same time as samples are run; normalising to a long-term mean should be avoided. Data are best normalised to a turret mean, provided the number of standards run is five or more in order that statistical robustness is approached, otherwise normalisation should be to a short-term mean encompassing the interval of sample analysis.

Given the above, it seems that uncertainty over normalisation is a continuing problem for SIS. In the Cenozoic, inaccurate normalisation will result in inaccuracy in predicted age derived from any SIS reference curve. The error would be of a magnitude that is inversely proportional to the gradient of the slope of $^{87}Sr/^{86}Sr$ *versus* time. For example, with our new curve (Fig. 10), an arbitrary inaccuracy of 0.000 019 would give an error of 0.27 myrs at 17.4 Ma where the curve is steepest (at −0.000 078 per myrs). The error would be around 1.1 myrs at 12.0 Ma where the gradient is lower (at −0.000 017 per myrs). These figures emphasise that control of standards is a key to accurate dating or correlation using Sr-isotope stratigraphy, yet few laboratories report $^{87}Sr/^{86}Sr$ for more than one standard, so our knowledge of residual bias is poor.

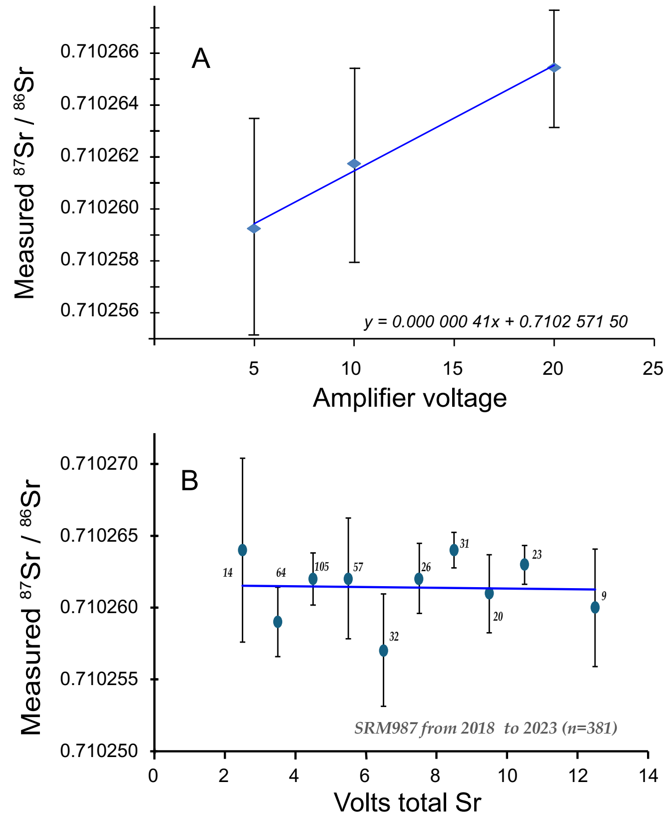

Fig. 6. A, possible relation between measured $^{87}Sr/^{86}Sr$ and amplifier voltage ($^{88}Sr^{+}$ ion-beam current) on a Triton MS at RIHN (Ando et al., 2010; modified from their Fig. 3). B. Absence of a relation between measured-$^{87}Sr/^{86}Sr$ and amplifier voltage on the Triton MS at NEIF in the period 2018 to 2023. Numbers in B refer to number of SRM987 standards aggregated for each data point.

The $^{87}Sr/^{86}Sr$ of standards used should be close to that of the samples being analysed, so the most appropriate standard for use in Sr-isotope stratigraphy for most of Phanerozoic time is E&A, with EN-1 best for Neogene and Cambrian samples. Unfortunately, neither E&A nor EN-1 seem to be widely available. A substitute for EN-1 is a modern calcite shell from an open-ocean locality well away from river influences *e.g.* a brachiopod, coral, or a nautilus obtained as bycatch in a fishery. Such carbonate standards match the matrix of most samples used in SIS and pass through columns during sample preparation, thereby providing a realistic measure of the precision on sample analysis. The standards JCp-1 (modern porites coral)and JCt-1 (modern *Tridacna* giant clam), originally distributed by the Geological Survey of Japan are no longer exported from Japan and the standards USGS MACS-3 (≈ 0.707 55) and USGS COQ-1 (≈ 0.703 3) are poorly characterised for $^{87}Sr/^{86}Sr$ and the latter is well below Phanerozoic values for marine-Sr.

4.3. The new reference curve for 11 to 20 Ma

Our new data for $^{87}Sr/^{86}Sr$ between 11 and 20 Ma, plotted to CENOGRID ages, define a curve (Fig. 8A) that is not smooth, so we first discuss the apparently discordant data highlighted as B, C, D and E, in Fig. 8A and then discuss the final calibration curve shown in Fig. 10 and tabulated in Table 3.

Data for U1338 (Fig. 8B) conform to a smooth curve but values of $^{87}Sr/^{86}Sr$ for U1338C-38H (three samples) and for U1338B-38H-4-W, 8-

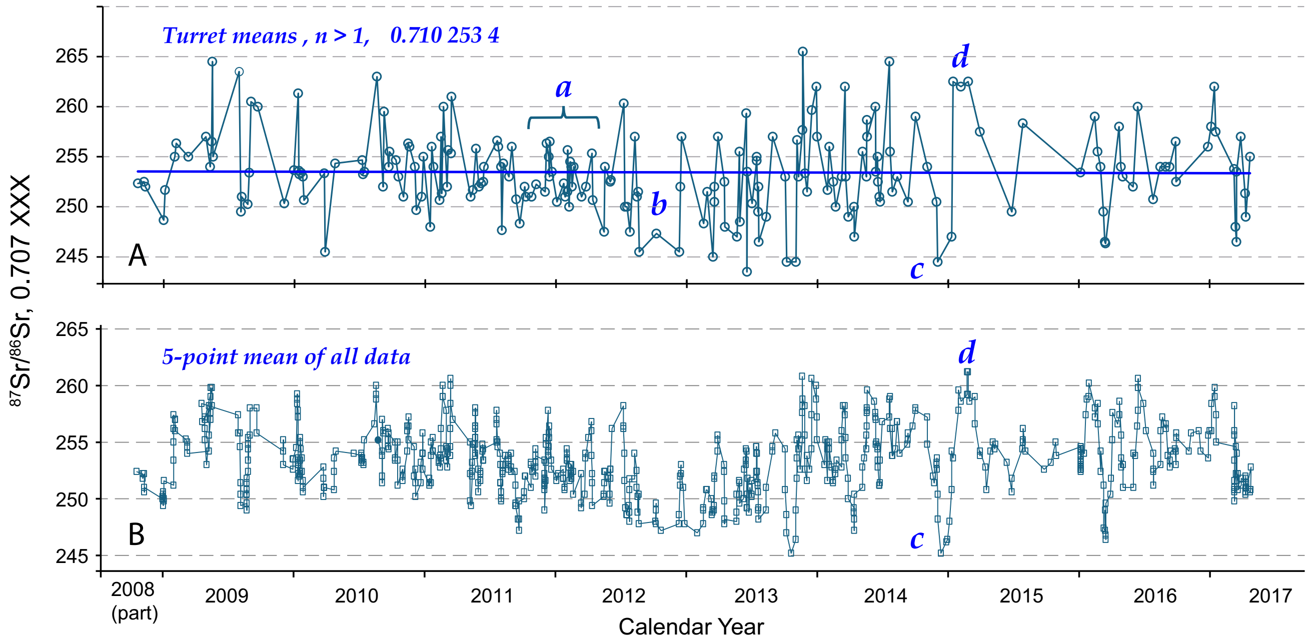

Fig. 7. Variation in measured $^{87}Sr/^{86}Sr$ of SRM987 over a 9-year period at NEIF. When more than one standard was run in a turret, values for turret means range from 0.710 245 to 0.710 265. A. All data. B. 5-point running mean of all data. Blue line in A is a linear regression fit with a slope of 0.000 000 2 over the 9 years shown. Variations in the $^{87}Sr/^{86}Sr$ of turret means are not random; there is a long-term minimum in 2012 – 2013. Other variations in part may reflect operator bias: at ***a***, 24 consecutive turrets show a variation of only ±0.000 003. At ***b***, three consecutive turrets fall 0.000 007 below the long-term mean. At ***c*** and ***d***, consecutive turrets fall 0.000 008 below and 0.000 010 above the mean. The data shown here were collected using the multidynamic algorithm of the Triton MS running mostly at 2 – 4 V signals for ^{88}Sr and runs of 60–100 cycles, rather than the 8 – 10 V signals and 300 – 600 cycles used in the present study. (For interpretation of the references to colour in this figure legend, the reader is referred to the web version of this article.)

10, all plot off the trend for the other data (Fig. 8C). Sample U1338C-38H-1-W, 122-124 is low by 0.000 005. This sample achieved only 175 measurements of $^{87}Sr/^{86}Sr$, rather than the typical 400, and was fractionated. The 2 s.e. on this sample was ±0.000 008, nearly three times the usual, and so this point does fall within uncertainty of the overall trend. This anomaly thus has an explanation. Sample U1338C-38H-3-W, 34-45 is high by 0.000 005; Sample U1338C-38H-5-W, 82-84 and U1338B-38H-4-W, 8-10 are both low by 0.000 009. The preservational state of these samples was as good as any we picked, so the anomalies cannot be attributed to poor preservation, a statement reinforced by the $^{87}Sr/^{86}Sr$ data for two samples from 1146A (48X-5-W, 12-14 cm, 49X–5-W, 145-147 cm) for which frosty planktic foraminifera were analysed (in the absence of alternative material): their $^{87}Sr/^{86}Sr$ values are concordant with data for other samples. Furthermore, for other samples, the scatter of $^{87}Sr/^{86}Sr$ about the regression line in Fig. 8B is no more than the precision of analysis of standards (typically ≤0.000 003, 2 s.e.), so, on that basis alone, samples were well preserved. Thus, no reason can be found for these three anomalies noted above but there may be significance in the fact that all are from Cores 38 of Holes B and C. As the $^{87}Sr/^{86}Sr$ of seawater cannot change on the timescale shown by these anomalies, they are treated henceforth as aberrant and are not used in any further analysis or plotting of our data. Good practice requires that these samples be re-prepared and re-analysed and that work is in progress.

The trends with time of $^{87}Sr/^{86}Sr$ for Sites 1146 and U1338 are discordant (Fig. 8C). Possible reasons for this offset are: 1) that errors were made in curating and sampling cores, so that we have not analysed samples from Site 1146; a test of this possibility is in progress. 2) the $^{87}Sr/^{86}Sr$ data is incorrect. The coherence and distinct patterns of the data suggests that this is unlikely, as do the repeat analysis undertaken. Furthermore, the profile of $^{87}Sr/^{86}Sr$ against depth for Site 1120 (Ando et al. (2011), which is shown in Fig. 9, has no break in slope at or near 12.7 Ma, which is at 110 mbsf. 3) $^{87}Sr/^{86}Sr$ decreases by 0.000 020 in the 0.1 myrs between 12.85 and 12.75 Ma. Such a change is incompatible with the residence time of Sr in the oceans (5.1 myrs in Broecker and Peng, 1982; 2.5 myrs in Hodell et al., 1990; 3.5 myrs in Lécuyer, 2016; 2.1 and 2.8 Ma quoted in Pearce et al., 2015), which is too long for such reversals to occur in the time available (Richter and Turekian, 1993). Put simply, the ocean's $^{87}Sr/^{86}Sr$ has too much inertia to change so sharply as the data imply. 4) the composite-depth model (missing or duplicated sediment) and/or astronomical calibration for either or both of Sites 1146 and U1338 have local inaccuracies.

At Site U1338, the bio-magneto-stratigraphic ages predicted by the age-model of Backman et al. (2016) agree to within 0.1 Ma with the astrochronometric ages for U1338 used in CENOGRID. This similarity reflects the fact that the U1338 astrochronology was built on the shipboard stratigraphy, which Backman et al. (2016) converted to the revised composite splice from Wilkens et al. (2013). No detailed later updates exist for the shipboard bio- and magnetostratigraphic datums, so future research in this area is warranted to verify these shipboard stratigraphic data. For instance, the magnetic record for Site U1338 is incomplete (Expedition 320/321 Scientists, 2010) and the Middle Miocene astrochronology at U1338 does not extend younger than 12.7 Ma, preventing better correlation with 1146, which does. At 1146, the composite splice and astrochronology have been revised as more stable isotope stratigraphies have become available (*e.g.*, Holbourn et al., 2018; Holbourn et al., 2024; De Vleeschouwer et al., 2020). Nonetheless, astrochronology and isotope stratigraphy ($\delta^{18}O$, $\delta^{13}C$) in this time interval is complex, as there are few records available globally that cover the Middle-Late Miocene continuously to help identify regional differences and potential hiatuses.

From the above, it is clear that further investigation is required to clarify the reason(s) for the discontinuity in age / $^{87}Sr/^{86}Sr$ between Sites 1146 and U1338. In the interim, and to construct our $^{87}Sr/^{86}Sr$ reference curve, we have recalculated the ages of Site 1146 using our $^{87}Sr/^{86}Sr$ data. We did so by fitting regression lines to data (Fig. 8C) and adding years to 1146-ages so that the regressions for 1146 superimposed exactly on the regression for U1338. The new ages for the interval 11 to

Table 3
Measured and normalised values of $^{87}Sr/^{86}Sr$ for microfossils from ODP/IODP Sites 1146, 1264, U1337, U1338. Normalised values are to 0.710 248 for SRM987. Age calibration is described in the text. The blue shading denotes ages used in this work. Period 1 was May – September 2023, Period 2 was February – May 2024; Period 3 was December, 2024 to February 2025.

Sample	Mean Depth CSF-A	Mean Depth rmcd	CENOGRID Age Ma	Backman *et al.* (2016) Bio-Mag Strat Age	$^{87}Sr/^{86}Sr$ Revised Age Ma	Hilgen 2025 Age Ma	Period	Measured $^{87}Sr/^{86}Sr$	Normalised to 248 $^{87}Sr/^{86}Sr$	± 2 s.e. ´10^{6}
1146A-46X-5-W, 29-31	430.80	459.84	11.055		11.251		2	0.708878	0.708871	2
1146C-46X-2-W, 65-67 (1)	432.76	462.20	11.154		11.414		1	0.708879	0.708865	2
1146C-46X-2-W, 65-67 (1)Rpt	432.76	462.20	11.154		11.414		3	0.708876	0.708866	2
1146C-46X-2-W, 65-67 (3)	432.76	462.20	11.154		11.414		1	0.708879	0.708865	2
1146C-46X-4-W, 0-2	435.11	464.55	11.252		11.573		1	0.708876	0.708862	2
1146A-47X-2-W, 29-31	435.90	466.94	11.354		11.740		2	0.708868	0.708861	3
1146A-47X-3-W, 90-92	438.01	469.05	11.456		11.906		2	0.708861	0.708854	2
1146A-47X-5-W, 144-146	441.55	472.59	11.653		12.228		2	0.708855	0.708848	2
1146C-47X-3-W, 109-111	444.30	474.80	11.752		12.390		1	0.708864	0.708850	4
1146C-47X-5-W, 41-43	446.62	477.12	11.857		12.561		1	0.708857	0.708843	2
1146A-48X-3-W, 109-111	447.80	479.13	11.957		12.725		2	0.708854	0.708847	3
1146A-48X-5-W, 10-12	449.81	481.14	12.052		12.879		2	0.708846	0.708839	2
1146A-48X-6-W, 62-64	451.83	483.16	12.152		13.043		2	0.708845	0.708838	3
1146C-48X-3-W, 134-136	454.15	484.86	12.265		12.946		1	0.708853	0.708839	2
1146C-48X-3-W, 134-136Rpt	454.15	484.86	12.265		12.946		3	0.708852	0.708842	2
1146C-48X-5-W, 49-51	456.30	487.01	12.357		13.101		1	0.708851	0.708837	2
1146C-48X-5-W, 49-51Rpt	456.30	487.01	12.357		13.101		3	0.708846	0.708836	2
1146A-49X-4-W, 79-81	458.75	489.01	12.450		13.529		2	0.708841	0.708834	2
1146A-49X-4-W, 79-81Rpt	458.75	489.01	12.450		13.529		2	0.708835	0.708828	2
1146A-49X-5-W, 145-147Rpt	460.91	491.16	12.553		13.697		2	0.708836	0.708829	2
1146A-49X-5-W, 145-147	460.91	491.16	12.553		13.697		2	0.708837	0.708830	3
1146C-49X-3-W, 79-81	463.30	493.41	12.658		13.611		1	0.708849	0.708835	2
1146C-49X-3-W, 79-81Rpt	463.30	493.41	12.658		13.611		3	0.708840	0.708830	2
1146C-49X-4-W, 133-135 (A)	465.34	495.45	12.757		13.778		1	0.708837	0.708823	2
1146C-49X-4-W, 133-135 (B)	465.34	495.45	12.757		13.778		1	0.708840	0.708826	2
U1338B-34H-2-W, 82-84	304.24	336.67	12.852	12.849			2	0.708850	0.708843	2
U1338B-34H-4-W, 62-64	307.05	339.48	12.958	12.923			2	0.708846	0.708839	2
U1338C-35H-3-W, 2-4	309.94	343.07	13.055	13.017			2	0.708842	0.708835	2
U1338B-35H-2-W, 52-54	313.43	347.21	13.160	13.126			2	0.708847	0.708840	3
U1338B-35H-4-W, 12-14	316.03	349.81	13.254	13.198			2	0.708842	0.708835	2
U1338C-36H-2-W, 72-74	318.63	353.20	13.342	13.310			2	0.708840	0.708833	2
U1338B-36H-2-W, 88-90	323.29	357.43	13.451	13.450			2	0.708840	0.708833	2
U1338B-36H-5-W, 7-9	326.98	361.12	13.553	13.573			2	0.708839	0.708832	2
U1338C-37H-2-W, 72-74	328.13	364.30	13.653	13.678			2	0.708834	0.708827	2
U1338B-37H-3-W, 2-4	333.43	368.61	13.753	13.821			2	0.708834	0.708827	2
U1338C-38H-1-W, 122-124#	336.63	373.42	13.861	13.981			2	0.708825	0.708818	8
U1338C-38H-3-W, 43-45#	338.84	375.63	13.952	14.054			2	0.708835	0.708828	3
U1338C-38H-5-W, 82-84#	342.23	379.02	14.057	14.166			2	0.708818	0.708811	2
U1338B-38H-4-W, 8-10#	344.49	381.57	14.150	14.251			2	0.708816	0.708809	3
U1338B-38H-4-W, 12-14	344.53	381.61	14.152	14.252			2	0.708822	0.708815	2
U1338C-39H-2-W, 62-64	347.03	384.33	14.257	14.342			2	0.708823	0.708816	2
U1338C-39H-4-W, 43-45	349.84	387.14	14.353	14.436			2	0.708819	0.708812	2
U1338C-39H-6-W, 27-29	352.68	389.98	14.451	14.530			2	0.708818	0.708811	2
U1338C-40H-2-W, 43-45	356.34	394.02	14.550	14.664			2	0.708815	0.708808	2
U1338C-40H-4-W, 83-85	359.74	397.42	14.653	14.776			2	0.708810	0.708803	2
U1338C-40H-6-W, 77-79	362.68	400.36	14.755	14.874			2	0.708804	0.708797	2
U1338B-40H-2-W, 29-33	360.71	403.11	14.848	14.965			2	0.708798	0.708791	2
U1338C-41H-5-W, 122-124	371.13	409.42	15.046	15.174			2	0.708790	0.708783	2
U1338B-41H-2-W, 100-102	370.91	414.58	15.252	15.327			2	0.708783	0.708776	2
U1338B-41H-4-W, 40-42	373.31	416.98	15.350	15.399			2	0.708776	0.708769	2
U1338C-43H-2-W, 18-20	379.59	420.04	15.434	15.491			2	0.708774	0.708767	2
U1338C-43H-4-W, 52-54	382.95	423.40	15.547	15.592			2	0.708764	0.708757	2

U1337A-35X-2-W, 74-76	321.15	349.82	15.567	15.759		2	0.708754	0.708747	3
U1337D-36X-3-W, 38-40	317.89	351.88	15.652		15.644	2	0.708761	0.708754	2
U1337D-36X-4-W, 76-78	319.77	353.76	15.757		15.734	2	0.708752	0.708745	2
U1337C-20X-5-W, 82-84	324.13	361.17	16.124			2	0.708725	0.708718	2
U1337C-20X-6-W, 80-82	325.61	362.68	16.192			2	0.708725	0.708718	2
U1337C-21X-2-W, 142-144	329.73	368.08	16.462		16.461	2	0.708705	0.708698	2
U1337C-21X-5-W, 64-66	333.45	371.80	16.657		16.704	2	0.708686	0.708679	2
U1337A-37X-3-W, 40-42	341.41	373.59	16.750	16.848		2	0.708673	0.708666	2
U1337A-37X-4-W, 74-76	343.25	375.43	16.852	16.928		2	0.708667	0.708660	3
U1337A-37X-5-W, 91-93	344.92	377.10	16.952	17.089		2	0.708655	0.708648	2
U1337C-22X-4-W, 0-2	340.91	380.58	17.149		17.249	2	0.708641	0.708634	2
U1337D-39X-3-W, 4-6	346.25	383.68	17.252		17.392	2	0.708630	0.708623	2
U1337D-39X-4-W, 144-146	349.15	386.58	17.351		17.521	2	0.708624	0.708617	2
U1337C-23X-3-W, 124-126	350.25	391.55	17.552		17.897	2	0.708597	0.708590	2
U1337D-40X-2-W, 114-116	355.45	393.56	17.655	18.092		2	0.708580	0.708573	2
U1337D-40X-3-W, 84-86	356.65	394.76	17.754	18.159		2	0.708575	0.708568	2
U1337D-40X-4-W, 60-62	357.91	396.02	17.852	18.252		2	0.708568	0.708561	3
U1337D-40X-5-W, 60-62	359.41	397.52	17.956	18.398		2	0.708557	0.708550	2
U1337C-24X-2-W, 144-146	358.55	399.30	18.054		18.428	2	0.708557	0.708550	2
U1337C-25X-4-W, 102-104		**412.65	18.803	18.930		3	0.708520	0.708510	2
U1337A-41X-2-W, 100-102		""416.40	19.013	19.116		3	0.708506	0.708496	2
U1337C-27X-2-W, 72-74		**432.22	19.601	19.620		3	0.708468	0.708458	2
U1337A-43X-6-W, 80-82		**443.10	19.989	20.030		3	0.708437	0.708427	3
1264A-20H-2-W, 119		205.92	17.245			3	0.708643	0.708634	2
1264A-20H-4-W, 59		208.32	17.724	17.825		3	0.708602	0.708593	2
1264A-20H-4-W, 88		208.61	17.807	18.065		3	0.708584	0.708575	2
1264A-20H-6-W, 34		211.07	18.292	18.412		3	0.708558	0.708549	3
1264B-21H-4-W, 74	193.04*	213.10	18.673			3	0.708539	0.708529	3
1264B-21H-5-W, 74	194.54*	214.60	18.899			3	0.708518	0.708508	2
1264A-21H-4-W, 23	194.53*	218.46	19.412			3	0.708485	0.708475	3
1264B-22H-5-W, 48	203.78*	224.53	20.093			3	0.708433	0.708423	2

Aberrant samples; not used for regressions * = mbsf **Table S31 of Westerhold et al. 2020

Aberrant samples; not used for regressions.
* = mbsf.
**Table S31 of Westerhold et al., 2020.

12.8 Ma on the cyclostratigraphic scale become 11.2 to 13.8 Ma on the Sr-isotope scale and both are shown in Table 3.

The new $^{87}Sr/^{86}Sr$-derived ages will be correct only if the ages for U1338 are correct, which will need confirming with future work. The new $^{87}Sr/^{86}Sr$-based chronology creates offsets in the stable $\delta^{18}O$ and $\delta^{13}C$ stratigraphies between Site 1146 and those of Sites U1337 and U1338 (Tian et al., 2018; Holbourn et al., 2022 and references therein). The new $^{87}Sr/^{86}Sr$-ages for Site 1146 disagree also with ages based on the shipboard biostratigraphic age model of Wang et al. (2000). We hypothesise that the location of Site 1146, in a marginal basin off the palaeo-Pearl River, introduced some diachroneity to fossil datums. In summary, the offset of up to 1 myr that we demonstrate between Sites 1146 and U1338 is currently without adequate explanation.

A second problem with the astronomical calibration of age underpinning CENOGRID occurs in the interval 16.7 to 20 Ma (Fig. 8D). In this interval, Miller et al. (2017) noted that some CENOGRID ages for U1337 might be wrong by 400 kyrs. Hilgen (2025) revised the ages for U1337 for the interval 15.5 to 18.7 Ma and suggested that the maximum error is around 300 kyrs. When our $^{87}Sr/^{86}Sr$ for U1337 is plotted to the CENOGRID timescale (Fig. 8D), the trend is dog-legged and incompatible with the residence time of Sr in the ocean. When plotted to our chosen ages (Table 3), the trend is smooth, effectively linear, essentially parallel to the LOWESS fit of McArthur et al. (2020), and is compatible with the residence time of Sr in the oceans. The trends overlap at ages younger than 16.5 Ma and diverge at older ages. In this work, we analysed samples from cores not included in Hilgen's revision of U1337 chronology. One of these was U1337D- 40X, Hilgen (2025) preferring its close correlative equivalent, U1337A-39X. Our $^{87}Sr/^{86}Sr$-ages for U1337D-40X are ≈ 400 kyrs older than CENOGRID ages (Table 3). Our data thus confirms the supposition of Miller et al. (2017) and Hilgen (2025) that some CENOGRID ages for U1337 are incorrect, and we show that they are incorrect between 16.5 and at least 20 Ma (Fig. 8D), rather than the 18.7 Ma at which the analysis of Hilgen (2025) was terminated.

A third problem arises in Site 1264. We analysed eight samples from this site, all from the interval in which age problems arise in U1337 (Fig. 8E). Five of these plot on the regression line in Fig. 8E whilst three, at ages younger than 18.5 Ma, plot below it *i.e.* show anomalously low ages. The age anomalies are up to 0.24 myrs and the samples are all low in $^{87}Sr/^{86}Sr$ by up to 0.000 020. Such aberrant data should not be accepted until confirmed by resampling and re-analysis: that is in progress and will be reported elsewhere. Notwithstanding that, the fact that the anomalies occur where ages for U1337 are most anomalous, and are also low, suggests that the anomalies are real. In the interim, we have added years to each of the three ages to bring them onto the regression line in Fig. 8E; the $^{87}Sr/^{86}Sr$-based ages are given in Table 3. If correct, these $^{87}Sr/^{86}Sr$- ages suggest that a local problem exists in the astrocalibration of Site 1264. Finally, when plotted to our chosen ages (Table 3) the regression line in Fig. 8 D,E, extrapolated to younger ages (Fig. 8F), fits better with U1338 data plotted to bio-magnetostratigraphy than when U1338 data is plotted to astrochronometric ages: this is one reason for our preferring to use the former over the latter in our final reference curve (Fig. 10).

Our $^{87}Sr/^{86}Sr$, plotted against our preferred ages (Table 3; Hilgen, CENOGRID) is shown in Fig. 10. The uncertainty of individual

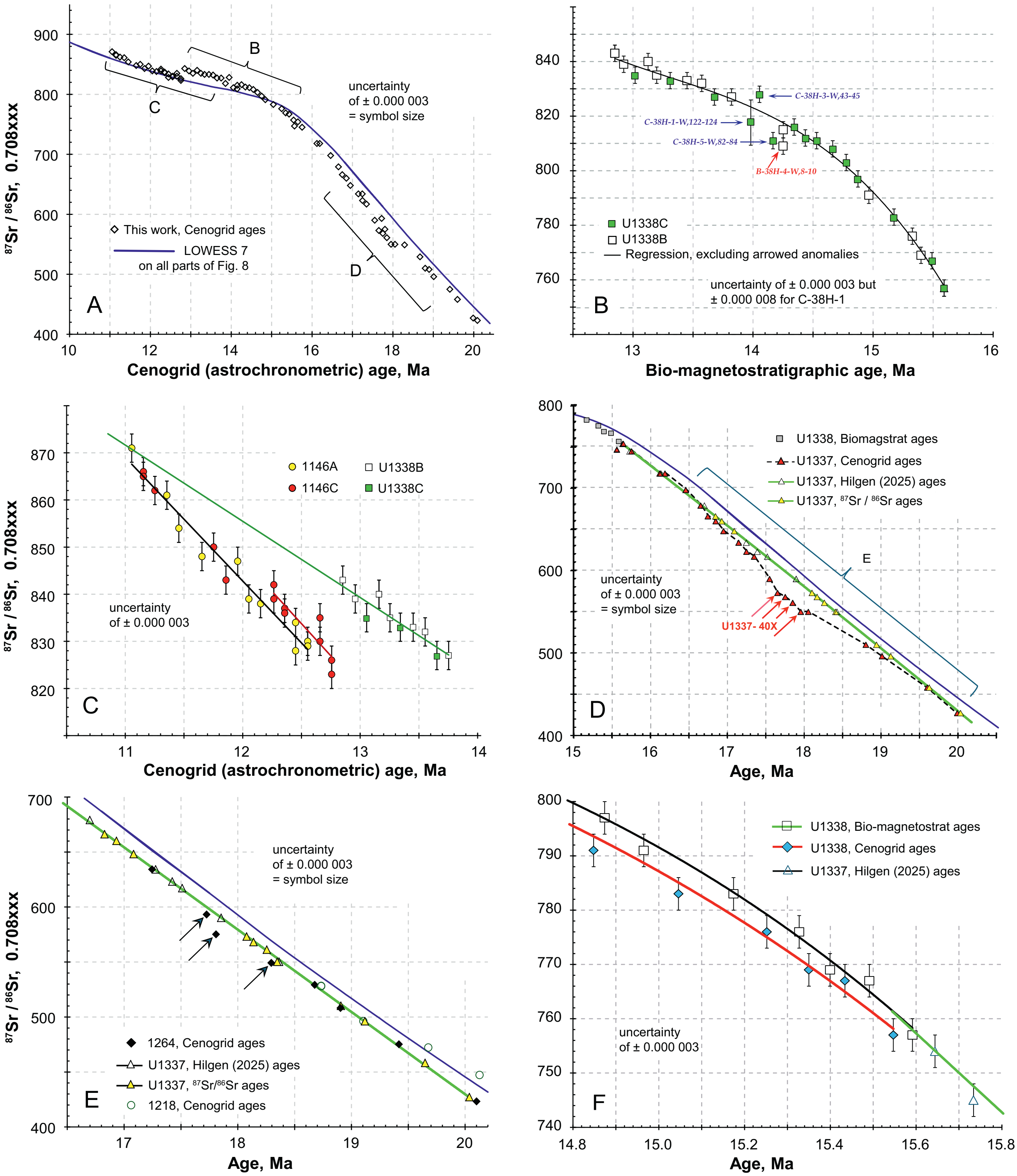

Fig. 8. Values of $^{87}Sr/^{86}Sr$ plotted against age. A. All data plotted to CENOGRID ages. Other plots show more detail of parts of the curve plotted to a range of timescales. CENOGRID ages and Hilgen (2025) ages are derived by astrochronology. The regression line in D and E is to our preferred ages that are listed in blue shading Table 3: It has the form Age = $-416{,}437.3460044860 \cdot R^2 + 576{,}816.21788458 \cdot R - 199{,}615.235613129$, where R = $^{87}Sr/^{86}Sr$ (see text for derivation). This regression was used to predict $^{87}Sr/^{86}Sr$-ages for samples that fall off the regression line and Hilgen ages were unavailable (Table 3). Arrows in D indicate samples from U1337-40X that have CENOGRID ages that appear low by 400 kyrs (Table 3). Arrows in E indicate three aberrant samples from 1264 for which $^{87}Sr/^{86}Sr$ ages were derived (Table 3). F. Intersection of the regression line shown in D and E, with the data trend from U1338 that is plotted against both the CENOGRID timescale and the bio-magnetostratigraphic timescale. of Backman et al. (2016).

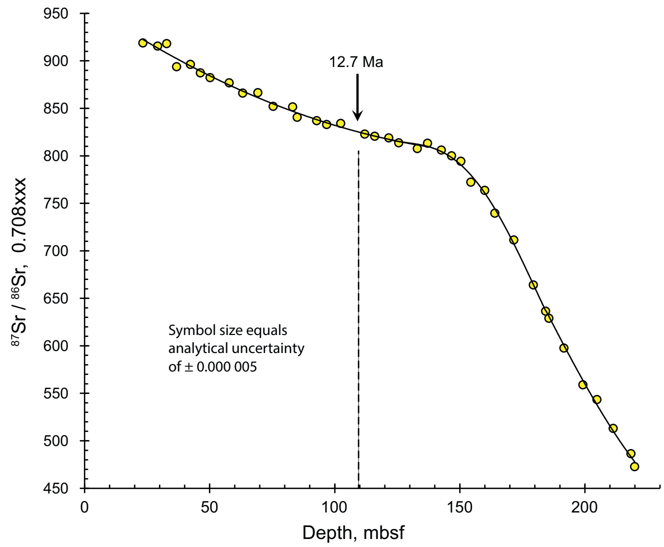

Fig. 9. Profile of $^{87}Sr/^{86}Sr$ against depth (mbsf) for Site 1120 (data of Ando et al., 2011). The data define a continuous smooth curve from 220 mbsf (19.4 Ma) to 23 mbsf (7.4 Ma). The age of 12.7 Ma occurs at 110 mbsf; there is no break in slope at or near that age (see Section 6 for more detail).

measurements of $^{87}Sr/^{86}Sr$ of our data are typically $\leq \pm$ 0.000 003 (Tables 1, 3). The uncertainty on the mean line, given in Table 3, is calculated as the standard error of the mean of blocks of 7 contiguous data-points. This uncertainty is less that the uncertainty on the distribution of data (given by 2 standard deviations), as we are concerned not with data distribution but the uncertainty of the position of the regression line. The data and mean line are unaffected by residual bias. Legacy data suffer from residual bias of around 0.000 020 (Oslick et al., 1994; Martin et al., 1999, Table 2). In order to improve SIS, further attention needs to be paid to better removing interlaboratory bias and residual bias and to developing new standards for $^{87}Sr/^{86}Sr$ analysis that match the values being measured.

Our sample ages are calibrated by bio-magnetostratigraphy (U1338), astrochronology and (minimally) $^{87}Sr/^{86}Sr$ chronology. The uncertainty in age is believed to be ≈ 0.1 Ma. Compared to a previous reference curve of McArthur et al. (McArthur et al., 2020; LOWESS 7, normalised to SRM987 of 0.710 248 and the timescale of Gradstein et al., 2020), our values of $^{87}Sr/^{86}Sr$ are higher by 0.000 020 at ages <15 Ma and lower by 0.000 015 at ages >15 Ma. These differences translate into differences in age of up to 0.2 Ma at ages >15 Ma where the curve is steep and up to 0.8 Ma at ages <15 Ma where it is shallow (Fig. 10). There is better agreement with the fit of McArthur et al. (2012, LOWESS 5, to the timescale of Gradstein et al., 2012), largely because LOWESS 5 did not include the data of Ando et al. (2011), which was to a chemostratigraphic age-model that gave ages too high by 0.9 Ma near 15 Ma (see Section 6 for details).

4.4. *A revised reference curve from 20 Ma to 32 Ma*

For all or part of the interval from 20 to 32 Ma, ocean drilling sites have been used to provide reference curves of $^{87}Sr/^{86}Sr$ against time by Palmer and Elderfield (1985; Sites 21 and 357, 0 – 75 Ma), DePaolo and Ingram (1985; 4 sites and land outcrops, 0 – 65 Ma), DePaolo (1986; Site 590B, 0 – 25 Ma), Hess et al. (1986; Sites 277, 305, 356, 366, 502, 516, 577, 593, 0 – 100 Ma), Miller et al. (1988; Site 522, 23 – 37 Ma), Miller et al., 1991, Hodell and Woodruff (1994; Sites 289 and 588, 6 – 26 Ma), Oslick et al. (1994 Site 747A, 10 – 25 Ma), Mead and Hodell (1995; Site 689B, 25 – 46 Ma), Zachos et al. (1992, 1999) and Reilly et al. (2002; Site 522, 23 – 35 Ma).

Some of the data in those publications, updated to the GTS2020 timescale, was used by McArthur et al. (2020) to generate an 'average' curve (LOWESS 7) for the interval. Subsequently, Stoll et al. (2023) have provided a further data-set and reference curve for the interval 18 – 32 Ma based on Site 1218 and using the astronomical age calibration from Pälike et al. (2006), updated in Westerhold et al. (2020; CENOGRID

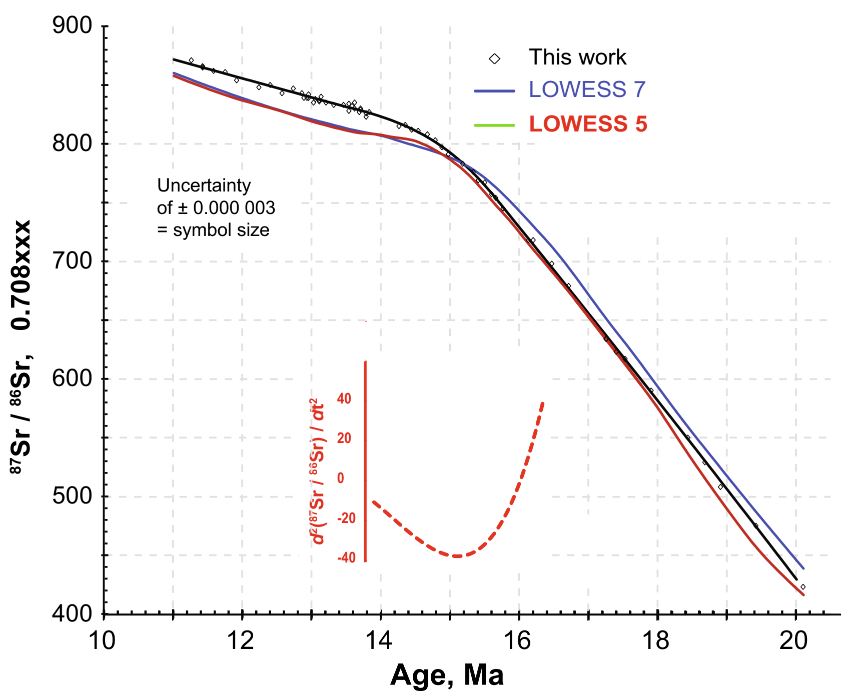

Fig. 10. Final reference curve of $^{87}Sr/^{86}Sr$ plotted against the age scale adopted here and compared to the reference curves of McArthur et al. (2012; LOWESS 5) and McArthur et al. (2020; LOWESS 7). Age derivation as described in the text. Ages derived from $^{87}Sr/^{86}Sr$ are not plotted. Red inset shows the second derivative of a 5th-order polynomial fit to data between 12.7 and 17.6 Ma used to determine that the precise point of inflection of the curve is at 15.1 Ma. (For interpretation of the references to colour in this figure legend, the reader is referred to the web version of this article.)

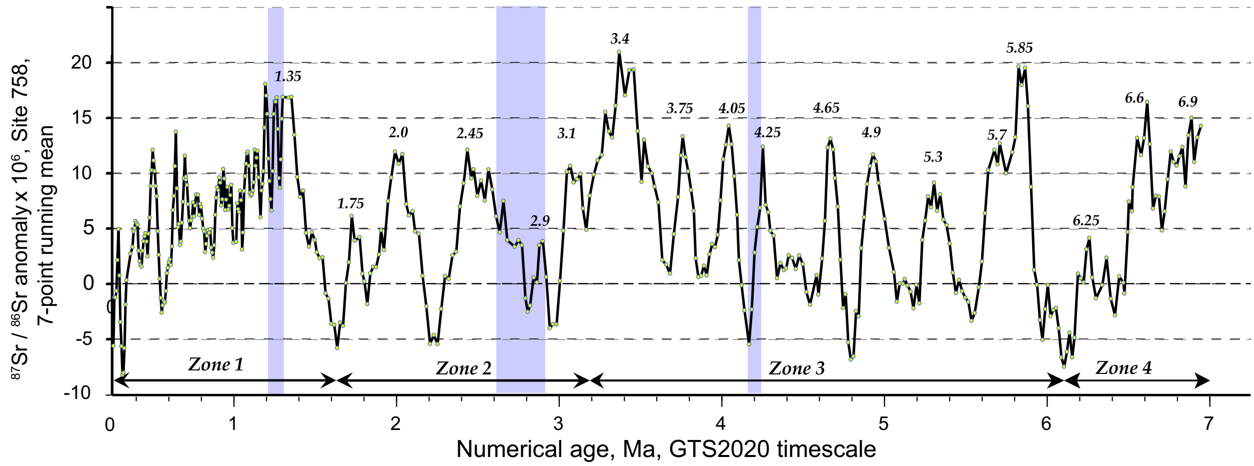

Fig. 11. The five-point running mean through the past 7 myrs of the difference between an open-ocean record of $^{87}Sr/^{86}Sr$ (this work) and the Site 758 record of $^{87}Sr/^{86}Sr$ from Farrell et al. (1995; *i.e.* FCG95). Data from FCG95 is normalised to SRM987 of 0.710 248 by subtraction of 0.000 009. For interpretation of Zone 1, 2, 3, 4, see text. The use of a 5-point mean displaces ages of peaks by up to 0.2 Ma. Blue shading indicates times of major changes identified by Sun et al. (2010) in the SE Asian monsoon. (For interpretation of the references to colour in this figure legend, the reader is referred to the web version of this article.)

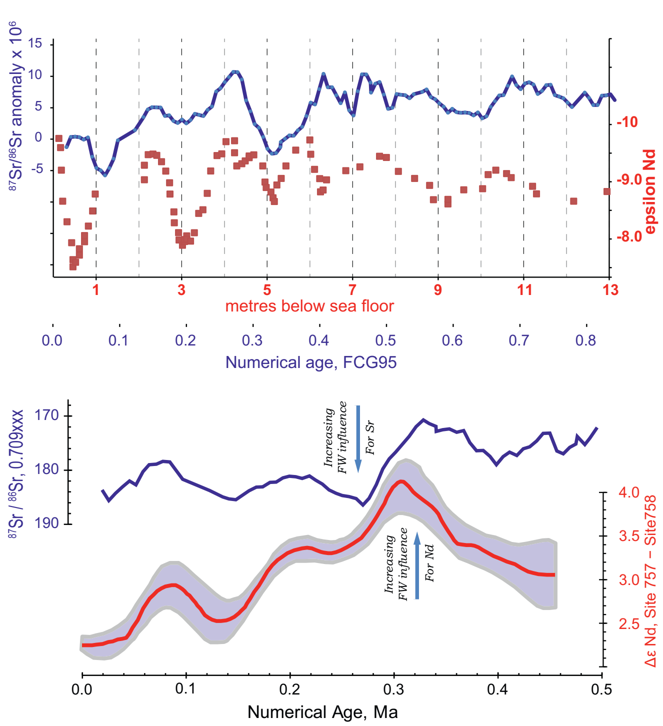

Fig. 12. A. Comparison of $^{87}Sr/^{86}Sr$-anomaly (blue line) from Fig. 11 and ξNd record (red squares) from Site 758. The $^{143}Nd/^{144}Nd$ record is from Gourlan et al. (2010) for foraminiferal calcite from ODP Site 758. Some co-variance is apparent between the trends for $^{87}Sr/^{86}Sr$ and $^{143}Nd/^{144}Nd$, albeit offset at some depths, possibly because FCG95 and Gourlan et al. (2010) used different depth scales. B. Comparison of 8-point running mean of the $^{87}Sr/^{86}Sr$ data of Farrell et al. (1995; note the inverted scale) for the freshwater-influenced Site 758 at 5°N in the southern Bay of Bengal and the isotopic difference in $^{143}Nd/^{144}Nd$ (expressed in epsilon notation) between ODP Site 758 and the fully-marine Site 757 at 17°S in the mid-Indian Ocean (adapted from Song et al., 2023). (For interpretation of the references to colour in this figure legend, the reader is referred to the web version of this article.)

ages). We have pruned the data of Stoll et al. (2023) to exclude four aberrant data (*e.g.* the two plotting above the LOWESS line in Fig. 8E) and used the rest to extend our curve to 32 Ma. For three reasons, our fit to the data of Stoll et al. (2023) does not honour putative slope changes or reversals in the curve proposed by those authors (*e.g.* reversals at ≈ 22.8 Ma, 26.5 Ma and 28.5 Ma). The changes are too sharp to be compatible with the residence time of Sr in the ocean (see Section 4.2). Moreover, the data defining the 'reversals' are few in number and analysis was not replicated to ensure the robustness of the data defining them. Finally, demonstrations of error and disparities (here and in Hilgen, 2025) in parts of the astrocalibrations of 1146, 1264, and U1337 (CENOGRID ages) makes hazardous the interpretation of such details in trends of $^{87}Sr/^{86}Sr$ plotted against astrocalibrated ages until more detailed integration has been achieved between $^{87}Sr/^{86}Sr$ and astrochronology at multiple sites.

4.5. Extending the reference curve from 11 Ma to 0 Ma

Curves of $^{87}Sr/^{86}Sr$ against time for all or part of the interval from 0 to 11 Ma, based mostly on ocean drilling sites, have been provided by Palmer and Elderfield (1985, Site 21 and 357, 0 – 75 Ma), DePaolo and Ingram (1985; 4 sites and land outcrops, 0 – 65 Ma), DePaolo (1986; Site 590B, 0 – 25 Ma), Hess et al. (1986; Sites 277, 305, 356, 366, 502, 516, 577, 593, 0 – 100 Ma), Richter and DePaolo (1988; Site 575 and 590B, 0 – 18 Ma), Hodell et al. (1989; Sites 502, 519, 588; 2 – 9 Ma), Capo and DePaolo (1990; 0 – 2.5 Ma), Hodell et al. (1990; Site 588, 607, 0 – 4 Ma), Miller et al. (1991; Site 608, 8 – 25 Ma), Hodell and Woodruff (1994; Sites 289 and 588, 6 – 26 Ma), Oslick et al. (1994 Site 747A, 10 – 25 Ma), Farrell et al. (1995; Site 758, 0 – 7 Ma), Martin et al. (1999; Site 926, 4 – 15 Ma), McArthur et al. (2006, Site 758 and Sicilian outcrop, 2 – 4.5 Ma).

Some of the data in those publications, updated to the GTS2020 timescale, were used by McArthur et al. (2020) to generate an 'average' curve for the Cenozoic, with most weight in the interval 0 to 7 Ma given to the data from Site 758 of Farrell et al. (1995; hereinafter FCG95) because of its high density of data and good age-model. Two problems with that data have now become apparent. The first is with normalisation; sample data were acquired in static mode whilst standard data (SRM987) were acquired in dynamic mode: the difference between static and dynamic data of FCG95 is 0.000 107, according to the SI of FCG95: adjusting across modes is unlikely to provide accurate normalisation. Normalising to data obtained on Holocene samples is also unwise because of the second problem affecting the data of FCG95.

The second problem is that FCG95 noted that their data showed "*high-frequency variations* (in $^{87}Sr/^{86}Sr$ that) *arise from some combination of analytical noise and natural variability*". FCG95 gave no explanation for the 'natural variability' they identified. Clemens et al. (1993), suggested that their record of $^{87}Sr/^{86}Sr$ in planktic foraminifera from Site 758 over

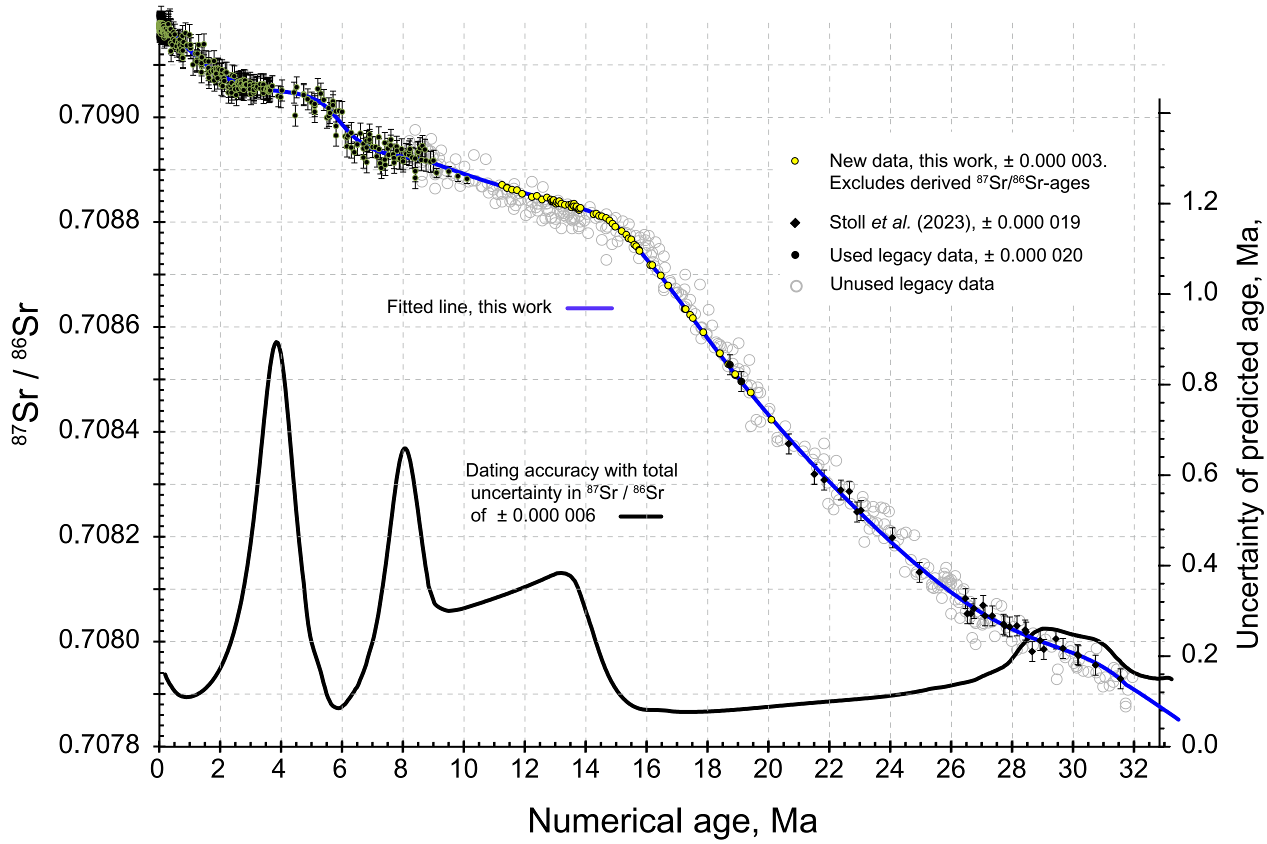

Fig. 13. New composite reference curve for 0 to 32 Ma (blue line). Data in Table 3 for which ages were derived from $^{87}Sr/^{86}Sr$ are not plotted. For clarity, uncertainty limits are not shown; they are given in Table 5. For legacy data at ages <10 Ma that is used here, uncertainty limits are shown at ±0.000 020 except for data of Ando et al. (2011) at ±0.000 005 ($n = 4$). Yellow circles are this work; symbol size equals the uncertainty (± 0.000 003). The uncertainty on the data of Stoll et al. (2023) s ±0.000 019. The black line is the uncertainty on prediction of agem with a total, arbitrary, uncertainty in $^{87}Sr/^{86}Sr$ of ±0.000 006 (combining uncertainty of reference line with uncertainty of measurement) and assuming no residual interlaboratory bias. Uncertainty in predicted age is inversely related to the slope of the reference curve. (For interpretation of the references to colour in this figure legend, the reader is referred to the web version of this article.)

Table 4
Sources used to fit the new reference curve of $^{87}Sr/^{86}Sr$ against time for the period 0 Ma to 11 Ma. Data in these sources were normalised to 0.710 248 for SRM987 and ages were updated to the timescale of Gradstein et al. (2020).

Source	Age range Used (Ma)
Ando et al. (2010)	0 – 0.14
Ando et al. (2011)	7 – 11
Capo and De Paolo (1990)	0 – 3.1
Dia et al. (1992)	0 – 0.26
Henderson et al. (1994)	0 – 0.27
Hodell et al. (1989)	2.0 – 8.8
Hodell et al. (1990)	0 – 4.1
Martin et al. (1999)	5.0 – 9.0
Mokadem et al. (2015)	0 – 0.04

the past 450 kyrs showed $^{87}Sr/^{86}Sr$ was higher in interglacial than in glacial times but gave no mechanistic explanation for the change. In contrast, Mokadem et al. (2015) found no such variations at Site 758 over the past 45 ka, a period that includes the last glacial maximum.

The natural variability identified by FCG95 persists and becomes clearer when the data is plotted as three-point, five-point, or seven-point, running means and so is likely to be real, as analytical noise should average to zero. In reality, it averages to signal, so we suggest that the natural variability is real and that it reflects riverine influences from the Ganges/Brahmaputra rivers. In Fig. 11, we plot a five-point running mean of the difference between the $^{87}Sr/^{86}Sr$ curve of FCG95 and our new curve; in doing so we use the original age-model of FCG95, based on Farrell and Janecek (1991) and updated to the GTS2020 timescale, rather than the age-models of Chen et al. (1995) or Ali et al. (2021).

The differences in Fig. 11 are mostly <0.000 020, yet they appear to demarcate four zones:

Zone 4 (7.0 – 6.1 Ma) is characterised by a decreasing baseline to a minima at 6.1 Ma, at which point riverine influences were presumed to be zero;

Zone 3 (6.1 – 3.2? Ma) by an increasing baseline to 3.2? Ma on which are superimposed 8 to 10 peaks, the number depending on whether the peaks at 5.7 Ma and 5.85 Ma are considered resolved, and whether one includes the peak at 3.1 Ma;

Zone 2 (3.2 – 1.6 Ma) by a return to a lower baseline three narrow and two broad peaks;

Zone 1 (1.6 – 0 Ma) by one broad peak (the numerous small peaks on its younger side, not seen on other peaks, reflect increased data density in this interval).

We advise caution in interpreting the magnitude of the variations, as the comparator is our new curve for the interval 0 – 7 Ma and that is based on literature data that has a precision lower than attainable today. Plainly, the variations in Fig. 11 need to be refined using a curve for 0 – 7 Ma that is based on new data with analytical uncertainties at the low end of what is currently attainable *i.e.* < 0.000 004. Nevertheless, we interpret the peaks and troughs in Fig. 11 as reflecting changes in $^{87}Sr/^{86}Sr$ of Sr in surface seawater at Site 758 over the past 7 myrs.

Such changes would have been driven by changing volumes of discharge of the Ganges-Brahmaputra / Meghna rivers, and their

Table 5
Values of marine $^{87}Sr/^{86}Sr$ through the last 32 myrs, tabulated in increments of time of 0.1 myrs. The uncertainty limits are mean deviations of data from the regression lines used to fit the data.

Age	$^{87}Sr/^{86}Sr$	2 s.e. $\times 10^6$	Age	$^{87}Sr/^{86}Sr$	2 s.e. $\times 10^6$	Age	$^{87}Sr/^{86}Sr$	2 s.e. $\times 10^6$	Age	$^{87}Sr/^{86}Sr$	2 s.e. $\times 10^6$	Age	$^{87}Sr/^{86}Sr$	2 s.e. $\times 10^6$
0.0	0.709174	4	7.0	0.708940	10	14.0	0.708823	1	21.0	0.708366	6	28.0	0.708023	4
0.1	0.709171	4	7.1	0.708937	8	14.1	0.708821	1	21.1	0.708360	6	28.1	0.708021	5
0.2	0.709167	4	7.2	0.708935	11	14.2	0.708819	1	21.2	0.708353	7	28.2	0.708018	6
0.3	0.709163	9	7.3	0.708933	14	14.3	0.708816	1	21.3	0.708347	6	28.3	0.708015	6
0.4	0.709159	10	7.4	0.708932	12	14.4	0.708814	1	21.4	0.708341	7	28.4	0.708013	6
0.5	0.709154	7	7.5	0.708930	11	14.5	0.708811	1	21.5	0.708335	7	28.5	0.708011	7
0.6	0.709149	6	7.6	0.708929	8	14.6	0.708808	1	21.6	0.708328	7	28.6	0.708008	8
0.7	0.709144	7	7.7	0.708928	10	14.7	0.708804	1	21.7	0.708322	7	28.7	0.708006	8
0.8	0.709139	11	7.8	0.708927	7	14.8	0.708801	1	21.8	0.708316	7	28.8	0.708004	8
0.9	0.709133	9	7.9	0.708926	7	14.9	0.708797	1	21.9	0.708310	7	28.9	0.708001	8
1.0	0.709128	7	8.0	0.708925	6	15.0	0.708792	1	22.0	0.708304	7	29.0	0.707999	7
1.1	0.709122	7	8.1	0.708924	7	15.1	0.708787	1	22.1	0.708298	7	29.1	0.707997	6
1.2	0.709117	7	8.2	0.708923	6	15.2	0.708782	1	22.2	0.708292	7	29.2	0.707995	6
1.3	0.709112	8	8.3	0.708922	11	15.3	0.708777	1	22.3	0.708286	7	29.3	0.707993	6
1.4	0.709107	7	8.4	0.708921	11	15.4	0.708771	1	22.4	0.708280	7	29.4	0.707991	6
1.5	0.709102	8	8.5	0.708920	10	15.5	0.708764	1	22.5	0.708275	7	29.5	0.707989	5
1.6	0.709097	8	8.6	0.708919	12	15.6	0.708757	1	22.6	0.708269	7	29.6	0.707986	4
1.7	0.709093	6	8.7	0.708918	9	15.7	0.708750	1	22.7	0.708263	7	29.7	0.707984	4
1.8	0.709089	5	8.8	0.708916	5	15.8	0.708743	1	22.8	0.708257	7	29.8	0.707982	4
1.9	0.709085	5	8.9	0.708914	6	15.9	0.708736	1	22.9	0.708251	7	29.9	0.707980	4
2.0	0.709081	6	9.0	0.708913	5	16.0	0.708728	1	23.0	0.708246	7	30.0	0.707978	4
2.1	0.709078	7	9.1	0.708910	5	16.1	0.708721	1	23.1	0.708240	8	30.1	0.707976	4
2.2	0.709075	9	9.2	0.708908	5	16.2	0.708714	1	23.2	0.708234	6	30.2	0.707973	4
2.3	0.709072	11	9.3	0.708906	5	16.3	0.708707	1	23.3	0.708229	7	30.3	0.707971	4
2.4	0.709069	8	9.4	0.708904	5	16.4	0.708699	1	23.4	0.708223	9	30.4	0.707968	4
2.5	0.709067	7	9.5	0.708902	6	16.5	0.708692	1	23.5	0.708218	7	30.5	0.707966	4
2.6	0.709065	3	9.6	0.708900	5	16.6	0.708685	1	23.6	0.708212	7	30.6	0.707963	4
2.7	0.709063	4	9.7	0.708898	5	16.7	0.708677	1	23.7	0.708207	7	30.7	0.707960	4
2.8	0.709061	3	9.8	0.708896	5	16.8	0.708670	1	23.8	0.708201	7	30.8	0.707957	4
2.9	0.709059	3	9.9	0.708894	5	16.9	0.708663	1	23.9	0.708196	7	30.9	0.707954	4
3.0	0.709058	5	10.0	0.708892	4	17.0	0.708655	1	24.0	0.708191	8	31.0	0.707951	4
3.1	0.709057	5	10.1	0.708890	4	17.1	0.708648	1	24.1	0.708185	8	31.1	0.707947	4
3.2	0.709056	2	10.2	0.708888	4	17.2	0.708640	1	24.2	0.708180	8	31.2	0.707943	4
3.3	0.709055	3	10.3	0.708886	4	17.3	0.708633	1	24.3	0.708175	8	31.3	0.707939	4
3.4	0.709054	4	10.4	0.708884	4	17.4	0.708626	1	24.4	0.708170	8	31.4	0.707935	4
3.5	0.709053	2	10.5	0.708882	4	17.5	0.708618	1	24.5	0.708164	8	31.5	0.707930	4
3.6	0.709052	2	10.6	0.708880	4	17.6	0.708611	1	24.6	0.708159	8	31.6	0.707925	4
3.7	0.709051	4	10.7	0.708878	3	17.7	0.708603	1	24.7	0.708154	8	31.7	0.707920	4
3.8	0.709051	5	10.8	0.708876	3	17.8	0.708596	1	24.8	0.708149	8	31.8	0.707915	4
3.9	0.709050	5	10.9	0.708875	3	17.9	0.708588	1	24.9	0.708144	7	31.9	0.707912	4
4.0	0.709049	4	11.0	0.708873	3	18.0	0.708581	1	25.0	0.708139	7	32.0	0.707908	4
4.1	0.709049	5	11.1	0.708871	3	18.1	0.708573	1	25.1	0.708135	7	32.1	0.707905	4
4.2	0.709048	5	11.2	0.708869	3	18.2	0.708566	1	25.2	0.708130	7	32.2	0.707901	4
4.3	0.709047	5	11.3	0.708867	3	18.3	0.708558	1	25.3	0.708125	6	32.3	0.707897	4
4.4	0.709046	4	11.4	0.708865	2	18.4	0.708551	2	25.4	0.708120	7	32.4	0.707893	4
4.5	0.709045	3	11.5	0.708864	1	18.5	0.708543	2	25.5	0.708116	7	32.5	0.707889	4
4.6	0.709044	4	11.6	0.708862	1	18.6	0.708536	2	25.6	0.708111	7	32.6	0.707885	4
4.7	0.709043	4	11.7	0.708860	1	18.7	0.708528	2	25.7	0.708107	7	32.7	0.707881	4
4.8	0.709041	6	11.8	0.708858	1	18.8	0.708521	2	25.8	0.708102	7	32.8	0.707877	4
4.9	0.709039	6	11.9	0.708857	1	18.9	0.708513	2	25.9	0.708098	7	32.9	0.707873	4
5.0	0.709036	6	12.0	0.708855	1	19.0	0.708506	1	26.0	0.708094	7	33.0	0.707869	4
5.1	0.709034	9	12.1	0.708854	2	19.1	0.708498	1	26.1	0.708089	7	33.1	0.707865	4
5.2	0.709031	11	12.2	0.708852	2	19.2	0.708490	1	26.2	0.708085	7	33.2	0.707861	4
5.3	0.709028	12	12.3	0.708851	2	19.3	0.708483	1	26.3	0.708081	7	33.3	0.707857	4
5.4	0.709023	9	12.4	0.708849	2	19.4	0.708475	1	26.4	0.708077	7	33.4	0.707853	4
5.5	0.709018	8	12.5	0.708847	2	19.5	0.708468	2	26.5	0.708073	8	33.5	0.707849	4
5.6	0.709013	9	12.6	0.708846	2	19.6	0.708460	2	26.6	0.708069	8			
5.7	0.709007	12	12.7	0.708844	2	19.7	0.708452	3	26.7	0.708066	7			
5.8	0.709000	14	12.8	0.708843	1	19.8	0.708446	3	26.8	0.708062	7			
5.9	0.708993	14	12.9	0.708841	2	19.9	0.708439	3	26.9	0.708058	6			
6.0	0.708986	15	13.0	0.708839	1	20.0	0.708432	4	27.0	0.708055	8			
6.1	0.708979	14	13.1	0.708838	1	20.1	0.708425	4	27.1	0.708051	4			
6.2	0.708973	11	13.2	0.708836	1	20.2	0.708418	4	27.2	0.708048	4			
6.3	0.708967	11	13.3	0.708834	1	20.3	0.708412	4	27.3	0.708044	3			
6.4	0.708962	10	13.4	0.708833	1	20.4	0.708405	4	27.4	0.708041	3			
6.5	0.708957	9	13.5	0.708831	1	20.5	0.708398	4	27.5	0.708038	3			
6.6	0.708953	10	13.6	0.708830	1	20.6	0.708392	5	27.6	0.708035	4			
6.7	0.708949	10	13.7	0.708828	1	20.7	0.708385	5	27.7	0.708032	4			
6.8	0.708946	12	13.8	0.708827	1	20.8	0.708379	5	27.8	0.708029	3			
6.9	0.708943	10	13.9	0.708825	1	20.9	0.708372	5	27.9	0.708026	4			

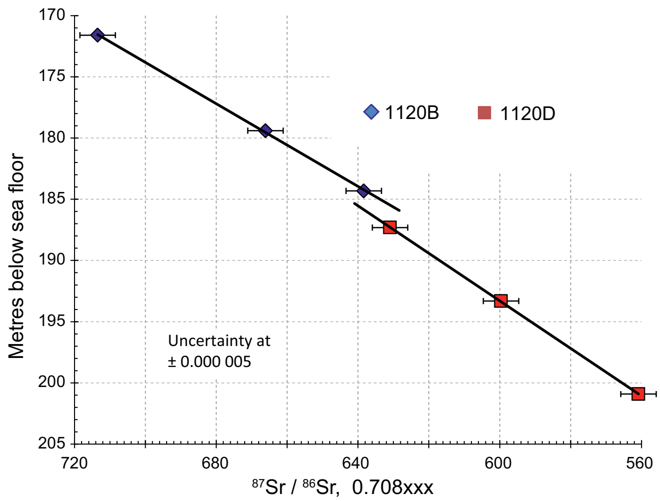

Fig. 14. Offset between Holes 1120B and 1120D when mbsf is plotted against the ^{87}Sr/^{86}Sr of Ando et al. (2011). This offset was corrected for here by subtracting 1.7 m from the depths of samples of Ando et al. (2011) from 1120D to make the mbsf for Hole D match Hole B, thus bringing both to a common depth scale.

dissolved-^{87}Sr/^{86}Sr, that both varied in time in response to climate-change that altered the duration and intensity of the Indian summer monsoon. Mixing that freshwater with seawater would have lowered the salinity of seawater and raised its ^{87}Sr/^{86}Sr with the effects decreasing with distance from the estuary. The question is then whether that influence would extend to Site 758.

Salinity is a proxy for riverine influence. Low-salinity coastal water is exported southwards in the Bay of Bengal by winter NE winds (Du and Zhang, 2016; Akhila et al., 2020; Podder et al., 2021) so it is no surprise that salinity variations on a glacial-interglacial timescale in the Bay of Bengal were noted by, *inter alia*, Cullen (1981) and Sijinkumar et al. (2016). On a shorter timescale, surface salinity variations in the vicinity of Site 758 range from ≈ 35 psu during the SW (summer) monsoon to ≈ 33.5 psu during the NE (winter) monsoon (Du and Zhang, 2016; Akhila et al., 2020; Podder et al., 2021). In modern times, extreme events have changed salinity by up to 4 psu (Chen et al., 2022) at Site 758.

Modelling also suggests that such changes in salinity are sufficient to affect ^{87}Sr/^{86}Sr at Site 758 today. The ^{87}Sr/^{86}Sr values in the present-day Ganges and Brahmaputra rivers are amongst the world's highest (Peucker-Ehrenbrink, 2018; Peucker-Ehrenbrink and Fiske, 2019), with annual discharge-weighted mean values of 0.728 and 0.720 respectively (Boral et al., 2021). Whilst the concentration of Sr in these rivers is inversely related to flow volume, even at maximum flow the concentrations of Sr and values of ^{87}Sr/^{86}Sr (Ganges >70 μg/l, ^{87}Sr/^{8} ^{6}Sr > 0.72; Brahmaputra >50 μg/l, ^{87}Sr/^{86}Sr > 0.718; Boral et al., 2021) in its water remain high enough to influence surface seawater in the southern Bay of Bengal. Using a two-end-member mixing model with a flux-weighted mean-annual concentration for the two rivers of 74 μg/l (*ibid*), the ^{87}Sr/^{86}Sr of seawater at Site 758 can be raised by 0.000 009 on reduction of salinity from 35 to 33 ‰, so the existence of such influences today is apparent. Given that Himalayan rivers may have had higher ^{87}Sr/^{86}Sr in the past (Quade et al., 1997) stronger influences in the past (Fig. 11) are feasible. Because FCG95 analysed planktic, rather than benthic, foraminifera, that riverine influence was preserved at Site 758, with the surface signal of low salinity and high ^{87}Sr/^{86}Sr being exported to deeper dwellers by dissolution of surface-derived *Acantharia* (Brass and Turekian, 1974; Steiner et al., 2020).

Evidence that riverine influences extended to Site 758 in the past derives further, albeit tentative, support from isotopic studies of neodymium (for a summary, see Song et al., 2023; Rashid et al., 2021). In brief, gradients of Nd-isotopic composition across the Bay of Bengal (Stoll et al., 2007; Singh et al., 2012) show that the influence of rivers on the isotopic composition of neodymium (ε_{Nd}) can extend to Site 758. As the neodymium isotope composition of foraminifera likely record benthic conditions (Roberts et al., 2012; Tachikawa et al., 2013), any riverine influence recorded by neodymium at Site 758 must be transmitted indirectly *via* sediment fractions (Song et al., 2023). Despite this indirect route, the ^{143}Nd/^{144}Nd record at Site 758 from planktic foraminifera show seasonal variations (Yu et al., 2017). Glacial-interglacial variations in ^{143}Nd/^{144}Nd (Burton and Vance, 2000; Gourlan et al., 2010) and in ^{187}Os/^{188}Os (Burton et al., 2010), at Site 758 have been

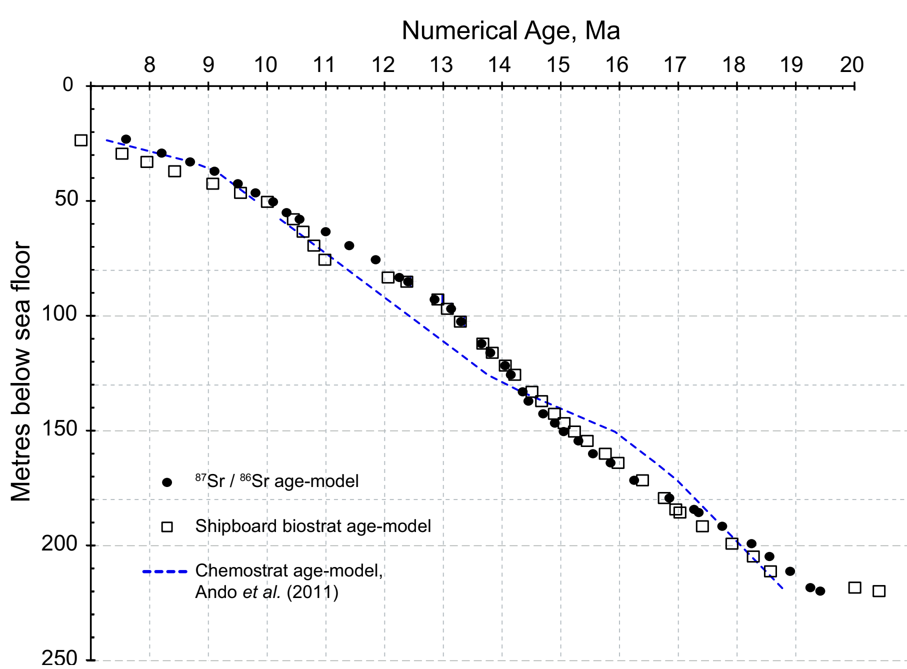

Fig. 15. Comparison of age-depth profiles according to three age-models for ODP Site 1120: the chemostratigraphic age-model of Ando et al. (2011); the shipboard age-model of Carter et al. (1999) updated to GTS2020; an age-model developed here from ^{87}Sr/^{86}Sr by assigning age to the ^{87}Sr/^{86}Sr of Ando et al. (2011) for Site 1120 using our new Neogene reference curve (Fig. 10, Table 5). The ^{87}Sr/^{86}Sr age-model for Site 1120 given in this figure is tabulated in Table 6.

Table 6
Age-depth models for IODP Site 1120. The column 'this work' is the model ages derived here from $^{87}Sr/^{86}Sr$ profile of Site 1120 and the new reference curve shown in Table 5 and Fig. 10. Levels above 36 mbsf are not defined by the new curve in Fig. 10 and so are speculative.

Sample	Depth (mbsf)	Unit[1]	$^{87}Sr/^{86}Sr$ to 248	Shipboard Berggren95 Ma	Shipboard GTS2020 Ma	This work Ma	Sedimentation Rate m/myrs
1120B-4H-1W, 100–103 cm	23.3	Unit III	0.708919	6.83	6.56	7.60	9.8
1120B-4H-5W, 100–103 cm	29.2	Unit III	0.708916	7.52	7.25	8.20	7.2
1120B-5H-1W, 100–103 cm	32.8	Unit III	0.708918	7.95	7.70	8.70	10.0
1120B-5H-4W, 50–53 cm	36.8	Unit III	0.708894	8.42	8.22	9.10	13.8
1120B-6H-1W, 100–103 cm	42.3	Unit III	0.708896	9.07	8.95	9.50	13.3
1120B-6H-4W, 50–53 cm	46.3	Unit III	0.708887	9.54	9.49	9.80	13.0
1120B-6H-6W, 140–143 cm	50.2	Unit III	0.708882	10.00	10.00	10.10	20.5
1120B-7H-3W	54.9	Base III				10.33	
1120B-7H-5W, 100–103 cm	57.8	Unit IV	0.708877	10.32	10.35	10.55	12.0
1120B-8H-2W, 140–143 cm	63.2	Unit IV	0.708866	10.49	10.54	11.00	15.3
1120B-9H-1W, 100–103 cm	69.3	Unit IV	0.708867	10.68	10.75	11.40	13.6
1120B-10X-2W, 130–133 cm	75.4	Unit IV	0.708852	10.87	10.96	11.85	19.5
1120B-11X-1W, 100–103 cm	83.2	Unit IV	0.708851	11.98	12.11	12.25	12.0
1120B-11X-2W, 130–133 cm	85.0	Unit IV	0.708841	12.31	12.44	12.40	17.3
1120B-12X-1W, 100–103 cm	92.8	Unit IV	0.708837	12.85	12.98	12.85	14.3
1120B-12X-4W, 50–53 cm	96.8	Unit IV	0.708833	13.01	13.14	13.13	32.9
1120B-13X-1W, 99–102 cm	102.4	Unit IV	0.708834	13.24	13.36	13.30	27.5
1120B-14X-1W, 100–103 cm	112.0	Unit IV	0.708823	13.63	13.74	13.65	26.7
1120B-14X-4W, 50–53 cm	116.0	Unit IV	0.708821	13.79	13.89	13.80	18.7
1120B-15X-1W, 100–103 cm	121.6	Unit IV	0.708819	14.02	14.11	14.10	26.7
1120B-15X-4W, 50–53 cm	125.6	Unit IV	0.708814	14.18	14.26	14.25	49.3
1120B-16X-2W, 139–142 cm	133.0	Unit IV	0.708808	14.48	14.54	14.40	27.4
1120B-16X-5W, 100–103 cm	137.1	Unit IV	0.708813	14.65	14.70	14.55	36.7
1120B-17X-2W, 140–143 cm	142.6	Unit IV	0.708806	14.87	14.91	14.70	20.5
1120B-17X-5W, 100–103 cm	146.7	Unit IV	0.708800	15.04	15.07	14.90	24.7
1120B-18X-1W, 100–103 cm	150.4	Unit IV	0.708794	15.22	15.24	15.05	17.4
1120B-18X-4W, 50–53 cm	154.4	Unit IV	0.708772	15.45	15.46	15.28	20.7
1120B-19X-1W, 100–103 cm	160.0	Unit IV	0.708764	15.78	15.77	15.55	13.3
1120B-19X-4W, 50–53 cm	164.0	Unit IV	0.708740	16.01	15.98	15.85	19.0
1120B-20X-2W, 140–143 cm	171.6	Unit IV	0.708711	16.46	16.40	16.25	13.0
1120B-21X-1W, 100–103 cm	179.4	Unit IV	0.708664	16.86	16.77	16.85	11.7
1120B-21X-4W, 140–143 cm*	184.3	Unit IV	0.708636	17.07	16.97	17.27	25.9
1120D-4X-1W, 100–103 cm**	185.6	Unit IV	0.708629	17.15	17.04	17.32	13.6
1120D-4X-5W, 100–103 cm**	191.6	Unit IV	0.708598	17.57	17.44	17.76	16.5
1120D-5X-4W, 50–53 cm**	199.2	Unit IV	0.708559	18.15	17.95	18.22	17.0
1120D-6X-1W, 100–103 cm**	204.8	Unit IV	0.708543	18.57	18.31	18.55	18.6
1120D-7X-2W, 140–143 cm**	211.3	Unit IV	0.708513	18.96	18.63	18.90	20.2
1120D-8X-4W, 50–53 cm**	218.4	Unit IV	0.708486	20.54	19.61	19.25	11.8
1120D-9X-2W, 140–143 cm**	219.9	Unit IV	0.708473	20.99	19.75	19.38	11.3

1. Units are those defined in Carter et al. (1999).
* mbsf corrected from 183.4.
** 1.70 m was subrtracted from mbsf of 1120D to correct for offset from 1120B.

demonstrated and may represent responses to varying riverine influence from the Ganges and Brahmaputra rivers. Furthermore, the $^{87}Sr/^{86}Sr$ record of FCG95 and the $^{143}Nd/^{144}Nd$ record at Site 758 over the past 0.8 Ma (Gourlan et al., 2010) show similar behaviour and departures from open-ocean values (Fig. 12A), although curve-matching is compromised by the different depth (and age) scales used by these authors. More tellingly, there is some concordance between the natural variability in $^{87}Sr/^{86}Sr$ at Site 758 and difference between the neodymium isotope compositions recorded at Site 758 and at Site 757; the latter is some 2300 km further south and so further from a Ganges influence (Fig. 12B; Song et al., 2023). Finally, Bretschneider et al. (Bretschneider et al., 2021; their Fig. 7) recorded a change in the $^{87}Sr/^{86}Sr$ of detrital clays that is co-incident in time with the monotonic rise in $^{87}Sr/^{86}Sr$ noted by Farrell et al. (1995) to have occurred between 6 and 5 Ma (Fig. 13). These coincidences support our view that the anomalies noted here in the $^{87}Sr/^{86}Sr$ record from Site 758 are real.

The monotonic increase noted by FCG95 in a 3-point mean of their data between 1.46 and 1.13 Ma is represented on Fig. 11 by the marked increase between 1.6 and 1.35 Ma, the age offset being a result of the use here of a five-point running mean. The steep increase slightly predates a marked change in the East Asian monsoon noted by Sun et al. (2010) to have occurred at 1.25 Ma. Other changes noted by Sun et al. (2010) at around 2.75 and 4.2 Ma do not appear on Fig. 11 to coincide with the zone boundaries identified here. The strengthening of the Indian summer monsoon between 5.8 and 5.2 Ma (Jöhnck et al., 2020) may be represented in Fig. 11 by the reversal in background slope from negative to positive around 6 Ma.

Given the above, a new reference curve is needed to replace the curve of FCG95. for marine-$^{87}Sr/^{86}Sr$ in the interval 0 to 7 Ma and to extend it to 11 Ma. Here we provide such a curve using sources listed in Table 4. For the interval 0 to 2 Ma, data were normalised by fitting linear or second-order regressions and adding or subtracting values sufficient to superimpose the regression curves and make the regression intercept 0.709 174 at 0 Ma. Other data was normalised to SRM987, excepting that of Martin et al. (Martin et al., 1999, Table 4) which plots around 0.000 012 lower than our data, after normalisation using their value of 0.710 235 for SRM987. We assume this difference represents residual bias, so we added 0.000 012 to that data to remove it.

5. The combined reference curves

We combine all of the above into one composite curve from 0 to 32 Ma (Fig. 13) that is tabulated in Table 5 at intervals of 0.1 Ma. The curve is a combined fit of separate but overlapping polynomial regressions. In

Fig. 13, for legacy data, *i.e.* data with ages <8 Ma, we show uncertainty bars of ±0.000 020 to represent the typical uncertainty quoted in original publications. For our data in Fig. 13, the size of the symbol denotes the uncertainty on values of $^{87}Sr/^{86}Sr$ (± 0.000 003). The uncertainty on the data of Stoll et al. (2023) is ±0.000 019.

The shape of the curve is close to previous published curves but in the interval 11 to 20 Ma has substantially smaller uncertainties in $^{87}Sr/^{86}Sr$ than previous data, Ando et al. (2011) apart. The uncertainty on the mean line is calculated as the standard error of the mean over blocks of 7 contiguous data-points. The uncertainties are not shown on Fig. 13 for clarity, but are given in Table 5. When using the curve to predict age for unknowns, the uncertainty of measurement of $^{87}Sr/^{86}Sr$ must be combined with the uncertainty of the mean line in order obtain a full estimate of uncertainty on predicted age.

The uncertainty on the position of the composite fitted line is less that the uncertainty on the distribution of data (given by 2 standard deviations), as we are concerned not with data distribution but the uncertainty of the position of the composite regression line. The data of Ando et al. (2011) and Stoll et al. (2023) are assumed not to be affected by residual bias. Legacy data (ages <11 Ma) may suffer from residual bias of around 0.000 020 (Oslick et al., 1994; Martin et al., 1999, Table 3) but its magnitude cannot be assessed accurately either because of a lack of relevant data, or because relevant data introduces conflict.

6. A new age-model for ODP Site 1120, 9.2 – 19.7 Ma

We use our new reference curve to refine the age model for ODP Site 1120B/D (Carter et al., 1999). For that site, Ando et al. (2011) provide a depth-profile of $^{87}Sr/^{86}Sr$ with analytical uncertainties of around ±0.000 005 (Fig. 9). Those authors presented a new age-model for the site based on their $^{87}Sr/^{86}Sr$ and 5 chemostratigraphic calibration points. That age-model differed from that developed by the shipboard party (Carter et al., 1999). Both the shipboard and Ando et al. (2011) age models utilise the mbsf depth scale. A shipboard composite depth scale was presented in Carter et al. (1999), but no composite splice was provided for the late Miocene interval. In developing our new age-model for Site 1120, for consistency we used mbsf depths and corrected them for two errors in Ando et al. (2011) by reference to core-store records (1120B-21X-4W, 140–143 cm should be at 184.3 mbsf, not the 183.4 mbsf given. 1120B-21X-2W, 50–53 cm, not analysed for $^{87}Sr/^{86}Sr$, should be at 180.4 mbsf, not the 181.3 mbsf given). We additionally corrected for an offset in mbsf depths between Holes B and D at Site 1120 by profiling $^{87}Sr/^{86}Sr$ against depth in both holes and identifying the offset of 1.70 m between them (Fig. 14). This places the Ando data from Holes B and D onto a common depth scale and thus also demonstrating the power of $^{87}Sr/^{86}Sr$ to check the accuracy of core splices. Using our new reference curve of $^{87}Sr/^{86}Sr$ against age (Fig. 10, Table 5), we assigned new ages to each $^{87}Sr/^{86}Sr$ value of Ando et al. (2011). The result is a new age-depth model for Site 1120B/D that is shown in Fig. 15 and tabulated in Table 6.

The data of Ando et al. (2011) were normalised by those authors to a value for SRM987 of 0.710 250 but no analysis of EN-1 was provided, so residual bias, if present, cannot be identified. Nevertheless, data in Ando et al. (Ando et al., 2010, Table 1) obtained using the same mass spectrometer shows measured values of 0.710 250± <0.000 001 (2.s.e, n = 6) for SRM987 and 0.709 179 ± 0.000 001 (2 s.e., n = 6) for Holocene foraminifera. These data suggest that residual bias in the data of Ando et al. (2011) is no more than 0.000 007. As we cannot be sure that that possible bias applies to the data of Ando et al. (2011) we have ignored it in arriving at the new age model for Site 1120 but we have re-normalised that data to a value of 0.710 248 for SRM987.

The age-model derived here from $^{87}Sr/^{86}Sr$ differs only a little from the biostratigraphic age-model of the shipboard party (Carter et al., 1999), updated to the Gradstein et al. (2020) timescale. Both age models differ from the age-model derived by Ando et al. (2011), mainly because those authors assigned an age of 15.9 to their calibration point 3, the point in the Middle Miocene where the high rate of change of $^{87}Sr/^{86}Sr$ in the Early Miocene switched to a lower rate in the Late Miocene. Here we show that the mid-point of that change was at 15.1 Ma.

7. Climate and the marine-$^{87}Sr/^{86}Sr$ record

Numerous articles have sought to explain why the marine-$^{87}Sr/^{86}Sr$ record shows such sinuosity; for recent discussions on the topic see, *inter alia*, Coogan and Dosso (2015), Peucker-Ehrenbrink and Fiske (2019), Gernon et al. (2021) and references therein. The drivers of the inflection between 16.0 and 13.6 Ma has received less attention, so a brief comment is in order in relation to glaciation. To give context, we show in Fig. 16 our record of $^{87}Sr/^{86}Sr$ alongside the CENOGRID record of marine $\delta^{18}O$ and marine $\delta^{13}C$ (Westerhold et al., 2020) and the period commonly termed the Miocene Climatic Optimum (Holbourn et al., 2015). The $^{87}Sr/^{86}Sr$ record from 25 Ma to 9 Ma (Fig. 13) consists of two straight lines connected by one inflection with a duration of 2.4 myrs. The slope of the $^{87}Sr/^{86}Sr$ record begins to decrease at 16.0 Ma; given the inertia to change of marine $^{87}Sr/^{86}Sr$ (Richter and Turekian, 1993) the forcing mechanism must have begun before that time – probably between 0.2 to 1 myrs beforehand; explanations of the change must account for that fact.

Explanations of the change-in-slope have included a wet-base to dry-based transition of Antarctic ice-sheets (*cf.* Zachos et al., 1999), and stabilization of the East Antarctic ice-sheet (Oslick et al. (1994). The past few decades of research, however, have revealed large scale oscillations in the size of Antarctic ice-sheets (Gasson et al., 2016; Miller et al., 2020;

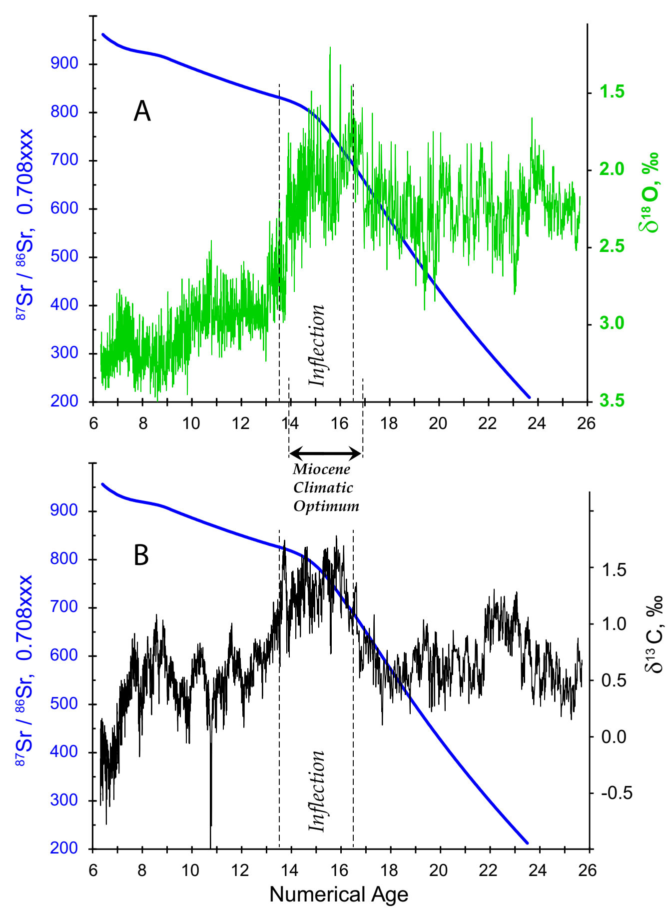

Fig. 16. Comparison of the Miocene record of $^{87}Sr/^{86}Sr$ with the record of $\delta^{18}O$ (A) and $\delta^{13}C$ (B) in benthic foraminiferal calcite. The limits of 16.0 Ma and 13.6 Ma for the start and end of the inflection are defined by the first differential of the 5th-order regression fit to $^{87}Sr/^{86}Sr$ data between 12.7 and 17.5 Ma.

Perez et al., 2021; Halberstadt et al., 2021; Klages et al., 2024, references therein, but *cf.* Balter-Kennedy et al., 2020) and such oscillations are not reflected in the simple curve presented in Fig. 13. The timing of such a wet-dry transition is uncertain beyond likely being younger than 15 Ma (*ibid*), and the thermal regime of the East Antarctic Ice-sheet was likely to have been geographically variable and, in places, warm-based or polythermal until ≈ 7 Ma (Smellie et al., 2014). Furthermore, Mokadem et al. (2015) showed that the marine-$^{87}Sr/^{86}Sr$ record for the past 45 ka, measured at a precision of ±0.000 005, showed no change relatable to glacial-interglacial cycles (*cf.* Blum and Erel, 1995). In short, the Sr-isotope trend in the Miocene is not easily relatable to events in Antarctica. Alternative explanations for the inflection in the $^{87}Sr/^{86}Sr$ trend at 15 Ma include eruption and weathering of Columbia River basalts (Hodell and Woodruff, 1994; Taylor and Lasaga, 1999), which appears incompatible with the monotonic increase in $^{87}Sr/^{86}Sr$ after 13.6 Ma, and increase in the supply of low-ratio Sr from emerging juvenile terrains since 15 Ma such as the SE Asian archipelago (Park et al., 2021), which might.

8. Implications and applications of high-precision SIS

Along with the work of Mokadem et al. (2015) and Ando et al. (2011), this work shows that analysis of $^{87}Sr/^{86}Sr$ can be done, with well-preserved samples, to a precision that will allow major problems of dating in the marine realm to be tackled. The accuracy of core composite-depths and splices, and astronomic calibrations, can be checked and improved using $^{87}Sr/^{86}Sr$ analysis. Synchroneity and diachroneity of fossil datums (*c.f.* Hess et al., 1989) can now be determined to an accuracy of around 0.1 Ma in the Oligocene and early-to-middle Miocene. Perhaps most importantly, this work suggests that it has been analytical matters, rather than problems of sample preservation, that have contributed most to the scatter of legacy $^{87}Sr/^{86}Sr$ and so reduced its ability to date well in the Neogene. We deduce this because, whilst the overwhelming majority of our samples were well preserved, two comprised >85 % of frosty planktic foraminifera, which many would regard as not preserved well. Yet these two samples have $^{87}Sr/^{86}Sr$ values concordant with other data, suggesting that the effects of such diagenetic alteration has little effect on $^{87}Sr/^{86}Sr$, whilst undoubtedly altering some proxy signals (Edgar et al., 2015). The principal problem that will compromise all of the above is interlaboratory bias, and that can be addressed through interlaboratory calibration exercises, analysis of more standards per sample and more than one standard, and development of additional standards specific to SIS.

9. Summary

1. We provide a new reference curve of $^{87}Sr/^{86}Sr$ *versus* time for the interval 0 to 32 Ma for use in correlation and dating with $^{87}Sr/^{86}Sr$. The interval 0 – 11 Ma is based on literature data with low-precision measurement of $^{87}Sr/^{86}Sr$, compared to that attainable today, so needs improving.
2. Dating and correlation with $^{87}Sr/^{86}Sr$ is hampered by residual bias in the measurement of $^{87}Sr/^{86}Sr$. Reporting values of $^{87}Sr/^{86}Sr$ for 2 or more standards would help eliminate this bias.
3. Sr-isotope stratigraphy has revealed apparent errors and discrepancies in the ages of [I]ODP cores dated by astrochronology. Most disparities between chronological approaches are <0.2 Ma but they range up to 1 Ma. Incorporating high-precision SIS into an integrated stratigraphic approach is now feasible to provide quality-control on astronomic calibrations of cores.
4. The natural variability of the $^{87}Sr/^{86}Sr$ record for 0 – 7 Ma of Farrell et al. (1995), for IODP Site 758 in the southern Bay of Bengal, provides a record of the intensity of the Indian summer monsoon.
5. Based on the new reference curve, we provide a new age-depth calibration for ODP Site 1120 (Campbell Plateau).
6. The rate of change of $^{87}Sr/^{86}Sr$ with time slows markedly between 16.0 and 13.6 Ma and is essentially linear for 5 myrs above and below these dates; nothing can be found in Antarctic glacial history that explain this shape of curve.

CRediT authorship contribution statement

J.M. McArthur: Writing – review & editing, Writing – original draft, Validation, Supervision, Resources, Project administration, Methodology, Investigation, Funding acquisition, Formal analysis, Data curation, Conceptualization. **I.L. Millar:** Writing – review & editing, Validation, Supervision, Methodology, Investigation, Funding acquisition, Formal analysis, Data curation. **A.J. Drury:** Writing – review & editing, Methodology, Investigation, Formal analysis, Data curation. **D. Wagner:** Data curation, Formal analysis, Investigation, Methodology, Validation.

Declaration of competing interest

The authors declare that they have no competing financial interests or personal relationships that might appear to influence the work reported in this paper.

Acknowledgements

The analysis presented here was supported by NERC/NEIF Project Grant 2022/2565. Drury was funded by the European Union's Horizon 2020 research and innovation programme under the Marie Skłodowska-Curie grant (agreement no. 796220) and the Royal Society (DHF\R1\221091). We thank Gianluca Frijia and an anonymous reviewer for their constructive comments. Jim Davy and Paul Minton kindly provided the photomicrographs in Fig. 3. We are grateful to S.A. Walker, Shellebarger Professor of Geology at the University of Georgia, and Douglas Dvoracek (deceased), University of Georgia, for encouragement that lead us to undertake this work. The Ocean Drilling Program and International Ocean Discovery Program provided the samples used in this study.

Appendix A. Supplementary data

Supplementary data to this article can be found online at https://doi.org/10.1016/j.palaeo.2025.112907.

Data availability

The data is where it should be - in the paper.

References

Akhila, V.P., Vialard, J., Lengaigneb, M., Keerthi, M.G., Boutin, J., Vergely, J.L., Papa, F., 2020. Bay of Bengal Sea surface salinity variability using a decade of improved SMOS re-processing. Remote Sens. Environ. 248, 111964.
Ali, S., Hathorne, E.C., Frank, M., 2021. Persistent provenance of South Asian monsoon-induced silicate weathering over the past 27 million years. Paleoceanog. Paleoclimatol. 36, 2020PA003909.
Ando, A., Nakano, T., Kawahata, H., Yokoyama, Y., Khim, B.-K., 2010. Testing seawater Sr isotopic variability on a glacial–interglacial timescale: an application of latest high precision thermal ionization mass spectrometry. Geochem. J. 44, 347–357.
Ando, A., Khim, B.-K., Nakano, T., Takata, H., 2011. Chemostratigraphic documentation of a complete Miocene intermediate-depth section in the Southern Ocean: Ocean Drilling Program Site 1120, Campbell Plateau off New Zealand. Mar. Geol. 279, 52–62.
Andrews, M.G., Jacobson, A.D., Lehn, G.O., Horton, T.W., Craw, D., 2016. Radiogenic and stable Sr isotope ratios (87Sr/86Sr, d88/86Sr) as tracers of riverine cation sources and biogeochemical cycling in the Milford Sound region of Fiordland. New Zealand. Geochim. Cosmochim.Acta 173, 284–303.
Backman, J., Baldauf, J.G., Ciummelli, M., Raffi, I., 2016. Data report: a revised biomagnetostratigraphic age model for Site U1338, IODP Expedition 320/321. In: Pälike, H., Lyle, M., Nishi, H., Raffi, I., Gamage, K., Klaus, A., The Expedition 320/321 scientists (Eds.), Proceedings of the Integrated Ocean Drilling Program, 320/321: Tokyo (IODP). https://doi.org/10.2204/iodp.proc.320321.219.2016.

Balter-Kennedy, A., Bromley, G., Balco, G., Thomas, H., Jackson, M., 2020. A 14.5million-year record of East Antarctic Ice Sheet fluctuations from the central Transantarctic Mountains, constrained with cosmogenic 3He, 10Be, 21Ne, and 26Al. Cryosphere 14, 2647–2672.
Blum, J.D., Erel, Y., 1995. A silicate weathering mechanism linking increases in marine ^{87}5r/^{86}5r with global glaciation. Nature 373, 415–418.
Boral, S., Peucker-Ehrenbrink, B., Hemingway, J.D., Sen, I.S., Galy, V., Fiske, G.J., 2021. Controls on short-term dissolved 87Sr/^{86} Sr variations in large rivers: evidence from the Ganga–Brahmaputra. Earth Planet. Sci. Letters 566, 116958.
Brass, G.W., Turekian, K.K., 1974. Strontium distributions in GEOSECS oceanic profiles. Earth Planet. Sci. Lett. 23, 141–148.
Bretschneider, L., Hathorne, E.C., Bolton, C.T., Gebregiorgis, D., Giosan, L., Gray, E., Huang, H., Holbourn, A., Kuhnt, W., Frank, M., 2021. Enhanced Late Miocene chemical weathering and altered precipitation patterns in the watersheds of the Bay of Bengal recorded by detrital clay radiogenic isotopes. Paleoceanography and Paleoclimatology 36 e2021PA004252.
Broecker, W.S., Peng, T.H., 1982. Tracers in the Sea. Lamont-Doherty Geological Observatory. Columbia University, Palisades, New York, 690pp.
Burke, W.H., Denison, R.E., Hetherington, E.A., Koepnick, R.B., Nelson, H.F., Otto, J.B., 1982. Variation of $^{87}Sr/^{86}Sr$ throughout Phanerozoic time. Geology 10, 516–519.
Burton, K.W., Vance, D., 2000. Glacial-interglacial variations in the neodymium isotope composition of seawater in the Bay of Bengal recorded by planktonic foraminifera. Earth Planet. Sci. Letters 176, 425–441.
Burton, K.W., Gannoun, A., Parkinson, I.J., 2010. Climate driven glacial–interglacial variations in the osmium isotope composition of seawater recorded by planktic foraminifera. Earth Planetary Sci. Letters 295 (1–2), 58–68.
Capo, R.C., DePaolo, D.J., 1990. Seawater strontium isotopic variations from 2.5 million years to the present. Science 249, 51–55.
Carter, R.M., McCave, I.N., Richter, C., Carter, L., et al., 1999. 4. Site 1120: central Campbell Plateau. Proceedings of the Ocean Drilling Program, Initial Reports Volume 181.
Chen, J., Farrell, J.W., Murray, D.W., Prell, W.L., 1995. Timescale and paleoceanographic implications of a 3.6 m.y. oxygen isotope record from the northeast Indian Ocean (Ocean Drilling Program site 758). Paleoceanography 10 (1), 21–47.
Chen, S., Cha, J., Qiu, F., Jing, C., Qiu, Y., Xu, J., 2022. Sea Surface salinity anomaly in the Bay of Bengal during the 2010 extremely negative IOD Event. Remote Sens. (Basel) 14, 6242.
Clemens, S.C., Farrell, J.W., Gromet, L.P., 1993. Synchronous changes in seawater strontium isotope composition and global climate. Nature 363, 607–610.
Coogan, L.A., Dosso, S.E., 2015. Alteration of ocean crust provides a strong temperature dependent feedback on the geological carbon cycle and is a primary driver of the Sr-isotopic composition of seawater. Earth Planet. Sci. Lett. 415, 38–46.
Cullen, J.L., 1981. Microfossil evidence for changing salinity patterns in the Bay of Bengal over the last 20 000 years. Palaeogeogr. Palaeoclimatol. Palaeoecol. 35, 315–356.
Dasch, D.J., Biscaye, P.E., 1971. Isotopic composition of Cretaceous-to-recent pelagic foraminifera. Earth Planet. Sci. Letters 11, 201–204.
De Vleeschouwer, D., Drury, A.J., Vahlenkamp, M., Rochholz, F., Liebrand, D., Pälike, H., 2020. High-latitude biomes and rock weathering mediate climate – carbon cycle feedbacks on eccentricity timescales. Nat. Commun. 11, 5013. https://doi.org/10.1038/s41467-020-18733-w.
DePaolo, D.J., 1986. Detailed record of the Neogene Sr isotopic evolution of seawater from DSDP Site 590B. Geology 14, 103–106.
DePaolo, D.J., Ingram, B.L., 1985. High-Resolution Stratigraphy with Strontium Isotopes. Science 227 (4689), 938–941.
Di, Y., Krestianinov, E., Zink, S., Amelin, Y., 2021. High-precision multidynamic Sr isotope analysis using thermal ionization mass spectrometer (TIMS) with correction of fractionation drift. Chem. Geol. 582, 120411.
Dia, A.N., Cohen, A.S., O'Nions, R.K., Shackleton, N.J., 1992. Seawater Sr isotope variation over the past 300 kyr and influence of global climate cycles. Nature 356, 786–788.
Drury, A.J., Liebrand, D., Westerhold, T., Beddow, H.M., Hodell, D.A., Rohlfs, N., Wilkens, R.H., Lyle, M., Bell, D.B., Kroon, D., Pälike, H., Lourens, L.J., 2021. Climate, cryosphere and carbon cycle controls on Southeast Atlantic orbital-scale carbonate deposition since the Oligocene (30–0 Ma). Clim. Past 17, 2091–2117.
Du, Y., Zhang, Y., 2016. Satellite and Argo observed surface salinity variations in the tropical Indian Ocean and their association with the Indian Ocean Dipole Mode 2016. J. Climate 28, 695–709.
Edgar, K.M., Anagnostou, E., Pearson, P.N., Foster, G.L., 2015. Assessing the impact of diagenesis on $\delta^{11}B$, $\delta^{13}C$, $\delta^{18}O$, Sr/Ca and B/Ca values in fossil planktic foraminiferal calcite. Geochim. Cosmochim. Acta 166, 189–209.
Expedition 320/321 Scientists, 2010. Site U1338. In Pälike H. Lyle M. Nishi H. Raffi I. Gamage K. Klaus A. and the Expedition 320/321 Scientists Proc. IODP 320/321: Tokyo. Integrated Ocean Drilling Program Management International, Inc. https://doi.org/10.2204/iodp.proc.320321.110.2010
Farrell, J.W., Janecek, T.R., 1991. Late Neogene paleoceanography and paleoclimatology of the northeast Indian Ocean (ODP Site 758). In: Proceedings, Ocean Drilling Program, Scientific Results, vol. 121. Ocean Drilling Program, College Station, Texas, pp. 297–355.
Farrell, J.W., Clemens, S.C., Gromet, L.P., 1995. Improved chronostratigraphic reference curve of late Neogene seawater $^{87}Sr/^{86}Sr$. Geology 23, 403406.
Fox, L.R., Wade, B.S., 2013. Systematic taxonomy of Early–Middle Miocene planktonic foraminifera from the equatorial Pacific Ocean: Integrated Ocean Drilling Program, Site U1338. J. Foraminifer. Res. 43 (4), 374–405.
Fox, L.R., Wade, B.S., Holbourn, A., Leng, M.J., Bhatia, R., 2021. Temperature gradients across the Pacific Ocean during the Middle Miocene. Paleoceanog. Palaeoclim. 36 e2020PA003924.
Gasson, E., DeConto, R.M., Pollard, D., Levy, R.H., 2016. Dynamic Antarctic ice sheet during the early to mid-Miocene. Proc. Natl. Acad. Sci. U. S. A. 113 (3), 3459–3464. https://doi.org/10.1073/pnas.1516130113.
Gernon, T.M., Hincks, T.K., Merdith, A.S., Rohling, E.J., Palmer, M.R., Foster, G.L., Bataille, C.P., Müller, R.D., 2021. Global chemical weathering dominated by continental arcs since the mid-Palaeozoic. Nat. Geosci. 14, 690–696. https://doi.org/10.1038/s41561–021-00806-0.
Gourlan, A.T., Meynadier, L., Allegre, C.J., Tapponnier, P., Birck, J.-L., Joron, J.-L., 2010. Northern Hemisphere climate control of the Bengali rivers discharge during the past 4 Ma. Quat. Sci. Rev. 29 (19–20), 2484–2498.
Gradstein, F.M., Ogg, J.G., Schmitz, M., Ogg, G. (Eds.), 2012. The Geologic Time Scale 2012. Boston, Elsevier. https://doi.org/10.1016/B978-0-444-59425-9.00004-4, 1176 p.
Gradstein, F.M., Ogg, J.G., Schmitz, M.D., Ogg, G.M., 2020. A Geologic Time Scale 2020, Vols. Elsevier, pp. 1357–pp.
Halberstadt, A.R.W., Chorley, H., Levy, R., Naish, T., De Conto, R.M., Gasson, E., Kowalewski, D.E., 2021. CO_2 and tectonic controls on Antarctic climate and ice-sheet evolution in the mid-Miocene. Earth Planet. Sci. Letters 564, 116908.
Henderson, G.M., Martel, D.J., O'Nions, R.K., Shackleton, N.J., 1994. Evolution of seawater $^{87}Sr/^{86}Sr$ over the last 400 ka: the absence of glacial/interglacial cycles. Earth Planetary Science Letters 128, 643–651.
Hess, J., Stott, L.D., Bender, M.L., Kennet, J.P., Schilling, J.-G., 1989. The Oligocene marine microfossil record: age assessments using strontium isotopes. Paleoceanog 4, 655–679.
Hilgen, F., 2025. Revised astrochronology for the Lower to Middle Miocene of IODP site U1337. Implications for the Cenozoic megasplice (CENOGRID). Palaeogeog. Palaeoclimatol. Palaeoecol. 662, 112748.
Hodell, D.A., Woodruff, F., 1994. Variations in the strontium isotopic ratio of seawater during the Miocene: stratigraphic and geochemical implications. Paleoceanography 9 (3), 405–426.
Hodell, D.A., Mueller, P.A., McKenzie, J.A., Mead, G.A., 1989. Strontium isotope stratigraphy and geochemistry of the late Neogene ocean. Earth Planet. Sci. Letters 92, 165–178.
Hodell, D.A., Mead, G.A., Mueller, P.A., 1990. Variation in the strontium isotopic composition of seawater (8 Ma to present): implications for chemical weathering rates and dissolved fluxes to the oceans. Chemical Geology (Isotope Geoscience Section) 80, 291–307.
Hodell, D.A., Mueller, P.A., Garrido, J.R., 1991. Variations in the strontium isotopic composition of seawater during the Neogene. Geology 19, 24–27.
Holbourn, A., Kuhnt, W., Kochhann, K.G.D., Andersen, N., Meier, K.J.S., 2015. Global perturbation of the carbon cycle at the onset of the Miocene Climatic Optimum. Geology 43, 123–126.
Holbourn, A.E., Kuhnt, W., Clemens, S.C., Kochhann, K.G.D., Jöhnck, J., Lübbers, J., Andersen, N., 2018. Late Miocene climate cooling and intensification of southeast Asian winter monsoon. Nature Comms 9, 1584. https://doi.org/10.1038/s41467-018-03950-1.
Holbourn, A., Kuhnt, W., Kochhann, K.G.D., Matsuzaki, K.M., Andersen, N., 2022. Middle Miocene climate–carbon cycle dynamics: Keys for understanding future trends on a warmer Earth? In: Aiello, I., Barron, J., Ravelo, C. (Eds.), Understanding the Monterey Formation and Similar Biosiliceous Units across Space and Time, Geol. Soc. Amer. Special Paper, vol. 556, pp. 1–20.
Holbourn, A., Kuhnt, W., Kulhanek, D.K., Mountain, G., Rosenthal, Y., Sagawa, T., Lübbers, J., Andersen, N., 2024. Re-organization of Pacific overturning circulation across the Miocene Climate Optimum. Nature Comms 15 (1). https://doi.org/10.1038/s41467-024-52516-x.
Jochum, K.P., Nohl, U., Herwig, K., Lammel, E., Stoll, B., Hofmann, A.W., 2007. GeoReM: a new geochemical database for reference materials and isotopic standards. Geostand. Geoanal. Res. 29 (3), 333–338. https://doi.org/10.1111/j.1751-908X.2005.tb00904.x.
Jöhnck, J., Khunt, W., Holbourn, A., Andersen, A., 2020. Variability of the Indiam monsoon in the Andaman Sea across the Miocene–Pliocene transition. Palaeoceanog Paleoclimatol. 35 e2020PA003923.
Klages, J.P., et al., 2024. Ice sheet free West Antarctica during peak early Oligocene glaciation. Science. https://doi.org/10.1126/science.adj3931.
Kochhann, K.G.D., Holbourn, A., Kuhnt, W., Channell, J.E.T., Lyle, M., Shackford, J.K., Wilkens, R.H., Andersen, N., 2016. Eccentricity pacing of eastern equatorial Pacific carbonate dissolution cycles during the Miocene Climatic Optimum. Paleoceanography 2016PA0029.
Lécuyer, C.C., 2016. Seawater residence times of some elements of geochemical interest and the salinity of the oceans. Bulletin de la Société Géologique de France 187 (6), 245–259.
Liebrand, D., Beddow, H.M., Lourens, J.L., Pälike, H., Raffi, I., Bohaty, S.M., Hilgen, F.J., Saes, M.J.M., Wilson, P.A., van Dijk, A.E., Hodell, D.A., Kroon, D., Huck, C.E., Batenburg, S.J., 2016. Cyclostratigraphy and eccentricity tuning of the early Oligocene through early Miocene (30.1–17.1 Ma): *Cibicides mundulus* stable oxygen and carbon isotope records from Walvis Ridge Site 1264. Earth Planet. Sci. Lett. 450, 392–405.
Ludwig, K.R., Halley, R.B., Simmons, K.R., Peterman, Z.E., 1988. Strontium-isotope stratigraphy of Enewetak Atoll. Geology 16 (16), 173–177.
Lyle, M., Drury, A.J., Tian, J., Wilkens, R., Westerhold, T., 2019. Late Miocene to Holocene high-resolution eastern equatorial Pacific carbonate records: stratigraphy linked by dissolution and paleoproductivity. Clim. Past 15 (5), 1715–1739.

Martin, E.E., Shackleton, N.J., Zachos, J.C., Flower, B.P., 1999. Orbitally-tuned Sr isotope chemostratigraphy for the late middle to late Miocene. Palaeoceanography 14, 74–83.

McArthur, J.M., 1994. Recent trends in strontium isotope stratigraphy. Terra Nova 6, 331–358.

McArthur, J.M., Rio, D., Massari, F., Castradori, D., Bailey, T.R., Thirlwall, M., Houghton, S., 2006. A revised Pliocene record for marine-$^{87}Sr/^{86}Sr$ used to date an interglacial event, Cockburn Island Formation, northern Antarctic Peninsula. Palaeogeog. Palaeoclimatol. Palaeoecol. 242, 126–136.

McArthur, J.M., Howarth, R.J., Shields, G.A., Zhou, Y., 2020. In: Gradstein, F.M., Ogg, J. G., Schmitz, M.D., Ogg, G.M. (Eds.), Sr-Isotope Stratigraphy, Chapter 7, Vol. 1, 211–238: *In*: A Geologic Time Scale 2020. Elsevier (2 Vols, 1357 pp).

Mead, G.A., Hodell, D.A., 1995. Controls on the $^{87}Sr/^{86}Sr$ composition of seawater from the middle Eocene to Oligocene: Hole-689B, Maud rise, Antarctica. Paleoceanography 10 (2), 327–346.

Miller, K.G., Feigenson, M.D., Kent, D.V., Olsson, R.K., 1988. Upper Eocene to Oligocene isotope ($^{87}Sr/^{86}Sr$, $\delta^{18}O$, $\delta^{13}C$) standard section, Deep Sea Drilling Project Site 522. Paleoceanography 3, 223–233. https://doi.org/10.1029/PA003i002p00223.

Miller, K.G., Feigenson, M.D., Wright, J.D., Clement, B.M., 1991. Miocene isotope reference section, Deep Sea Drilling Project Site 608: an evaluation of isotope and biostratigraphic resolution. Paleoceanography 445 (6), 33–52. https://doi.org/10.1029/90PA01941.

Miller, K.G., Baluyot, R., Wright, J.D., Kopp, R.E., Browning, J.V., 2017. Closing an early Miocene astronomical gap with Southern Ocean $\delta^{18}O$ and $\delta^{13}C$ records: Implications for sea level change. Paleoceanography 32, 600–621. https://doi.org/10.1002/2016PA003074.

Miller, K.G., Browning, J.V., Schmelz, W.J., Kopp, R.E., Mountain, G.S., Wright, J.D., 2020. Cenozoic sea-level and cryospheric evolution from deep-sea geochemical and continental margin records. Sci. Adv. 6 (20). https://doi.org/10.1126/sciadv.aaz1346.

Mokadem, F., Parkinson, I.J., Hathorne, E.C., Ananda, P., Allen, J.T., Burton, K.W., 2015. High-precision radiogenic strontium isotope measurements of the modern and glacial ocean: limits on glacial-interglacial variations in continental weathering. Earth Planet. Sci. Letters 415, 111–120.

Oslick, J.S., Miller, K.G., Feigenson, M.D., Wright, J.D., 1994. Oligocene–Miocene strontium isotopes: stratigraphic revisions and correlations to an inferred glacioeustatic record. Paleoceanography 9, 427–443. https://doi.org/10.1029/94PA00249.

Pälike, H., Norris, R.D., Herrle, J.O., Wilson, P.A., Coxall, H.K., Lear, C.H., Shackleton, N. J., Tripati, A.K., Wade, B.S., 2006. The heartbeat of the Oligocene climate system. Science 314, 1894–1898. https://doi.org/10.1126/science.1133822.

Palmer, M.R., Elderfield, H., 1985. Sr isotope composition of seawater over the past 75 Myr. Nature 314, 526–528.

Park, Y., Maffre, P., Godderis, Y., Macdonald, F.A., Anttila, E.S.C., Swanson-Hysella, N.L., 2021. Emergence of the Southeast Asian islands as a driver for Neogene cooling. Proc. Nat. Acad. Sci. 117 (41), 25319–25326.

Pearce, C.R., Parkinson, I.J., Gaillardet, J., Charlier, B.L.A., Mokadem, F., Burton, K.W., 2015. Reassessing the stable ($\delta^{88/86}Sr$) and radiogenic ($^{87}Sr/^{86}Sr$) strontium isotopic composition of marine inputs. Geochim. Cosmochim. Acta 157, 125–146.

Perez, L.F., et al., 2021. Early and middle Miocene ice sheet dynamics in the Ross Sea: results from integrated core-log-seismic interpretation. Geol. Amer. Sci. Bull. 134 (1/2), 348–370.

Peterman, Z.E., Hedge, C.E., Tourtelot, H.A., 1970. Isotopic composition of strontium in sea water throughout Phanerozoic time. Geochim. Cosmochim. Acta 34, 105–120.

Peucker-Ehrenbrink, B., 2018. Land2Sea Database, Version 2.0. Pangaea, 892680. https://doi.org/10.1594/PANGAEA.

Peucker-Ehrenbrink, B., Fiske, G.J., 2019. A continental perspective of the seawater $^{87}Sr/^{86}Sr$ record: a review. Chem. Geol. 510, 140–165. https://doi.org/10.1016/j.chemgeo.2019.01.017.

Podder, R.S.I.S., Gupta, A.K., Clemens, S., 2021. Surface paleoceanography of the eastern equatorial Indian Ocean since the latest Miocene: Foraminiferal census and isotope records from ODP Hole 758A. Palaeogeog., Palaeoclimatol., Palaeoecol. 579, 110617.

Podosek, F.A., Zinner, E.K., Macpherson, G.J., Lundberg, L.L., Brannon, J.C., Fahey, A.J., 1991. Correlated study of initial 87Sr/86Sr and Al-Mg isotopic systematics and petrologic properties in a suite of refractory inclusions from the Allende meteorite. Geochim. Cosmochim. Acta 55, 1083–1110.

Quade, J., Roe, L., DeCelles, G., Tank, P.O., 1997. The late Neogene 87Sr/86Sr record of lowland himalayan rivers. Science 276, 1828–1831.

Rashid, H., Wang, Y., Gourlan, A.T., 2021. Impact of climate change on past Indian monsoon and circulation: a perspective based on radiogenic and trace metal geochemistry. Atmosphere 12 (3). https://doi.org/10.3390/atmos12030330 art. no. 330.

Reilly, T.J., Miller, K.G., Feigenson, M.D., 2002. Latest Eocene-earliest Miocene Sr isotopic reference section, Site 522, eastern South Atlantic. Paleoceanography 17 (3), 1046. https://doi.org/10.1029/2001PA000745.

Richter, F.M., DePaolo, D.J., 1988. Diagenesis and Sr isotopic evolution of seawater using data from DSDP 590B and 575. Earth Planet. Sci. Lett. 90, 382–394.

Richter, F.M., Turekian, K.K., 1993. Simple models for the geochemical response of the ocean to climatic and tectonic forcing. Earth Planet. Sci. Lett. 119, 121–131.

Roberts, N.L., Piotrowski, A.M., Elderfield, H., Eglinton, T.I., Lomas, M.W., 2012. Rare earth element association with foraminifera. Geochim. Cosmochim. Acta 94, 57–71.

Schneider, J.M., Kleine, T., 2024. Effects of Faraday-cup deterioration on Sr and Cr isotope analyses by thermal ionization mass spectrometry. J. Anal. At. Spectrom. https://doi.org/10.1039/d4ja00153b.

Sijinkumar, A.V., Clemens, S., Nath, B.N., Prell, W., Benshila, R., Lengaigne, M., 2016. $\delta^{18}O$ and salinity variability from the Last Glacial Maximum to Recent in the Bay of Bengal and Andaman Sea. Quat. Sci. Rev. 135, 79e91.

Singh, S.S., Singh, S.K., Goswami, V., Bhushan, R., Rai, V.K., 2012. Spatial distribution of dissolved neodymium and εNd in the Bay of Bengal: Role of particulate matter and mixing of water masses. Geochim. Cosmochim. Acta 94, 38–56.

Smellie, J.L., Rocchi, S., Wilch, T.I., Gemelli, M., Di Vincenzo, G., McIntosh, W., Dunbar, N., Panter6 K., and Fargo A., 2014. Glaciovolcanic evidence for a polythermal Neogene East Antarctic Ice Sheet. Geology 42 (1), 39–41.

Song, Z., Wan, S., Colin, C., France-Lanord, C., Yu, Z., Dapoigny, A., Jin, H., Li, M., Zhang, J., Zhao, D., Shi, X., Li, A., 2023. Enhanced weathering input from South Asia to the Indian Ocean since the late Eocene 2023. Sci. Bull. 68, 305–313.

Steiner, Z., Sarkar, A., Prakash, S., Vinaychandran, P.N., Turchyn, A.V., 2020. Dissolved strontium, Sr/Ca ratios, and the abundance of *Acantharia* in the Indian and Southern Oceans. ACS Earth Space Chem. 4, 802–811.

Stoll, H.M., Vance, D., Arevalos, A., 2007. Records of the Nd isotope composition of seawater from the Bay of Bengal: Implications for the impact of Northern Hemisphere cooling on ITCZ movement. Earth Planet. Sci. Lett. 255 (1–2), 213–228.

Stoll, H.M., Pena, L.D., Hernandez-Almeida, I., Guitian, J., Tanner, T., Pälike, H., 2023. Nonlinear increase in seawater $^{87}Sr/^{86}Sr$ in the Oligocene to early Miocene and implications for climate-sensitive weathering. Clim. Past. https://doi.org/10.5194/cp-2023-29.

Sun, Y., An, Z., Clemens, S.C., Bloemendal, J., Vandenberghe, J., 2010. Seven million years of wind and precipitation variability on the Chinese Loess Plateau. Earth Planet. Sci. Lett. 297, 525–353.

Tachikawa, K., Toyofuku, T., Basile-Doelsch, I., Delhaye, T., 2013. Microscale neodymium distribution in sedimentary planktonic foraminiferal tests and associated mineral phases. Geochim. Cosmochim. Acta 100, 11–23.

Taylor, A.S., Lasaga, A.C., 1999. The role of basalt weathering in the Sr isotope budget of the oceans. Chem. Geol. 161, 199–214.

Thirlwall, M.F., 1991. Long-term reproducibility of multicollector Sr and Nd isotope ratio analysis. Chem. Geol. (Isot. Geosci. Sect.) 94, 85–104.

Tian, J., Ma, X., Zhou, J., Jiang, X., Lyle, M., Shackford, J., Wilkens, R., 2018. Paleoceanography of the east equatorial Pacific over the past 16 Myr and Pacific–Atlantic comparison: high resolution benthic foraminiferal $\delta^{18}O$ and $\delta^{13}C$ records at IODP Site U1337. Earth Planet. Sci. Lett. 499, 185–196.

USGS, 2024. https://www.usgs.gov/centers/gggsc/science/usgs-geochemical-and-microanalytical-reference-materials-distribution. Accessed on 31 12 2024.

Veizer, J., Compston, W., 1974. $^{87}Sr/^{86}Sr$ composition of seawater during the Phanerozoic. Geochim. Cosmochim. Acta 33, 1461–1484.

Wang, P., Prell, W.L., Blum, P., et al., 2000. Proceedings of the Ocean Drilling Program, Initial Reports 184, 101 pp. https://doi.org/10.2973/odp.proc.ir.184.107.2000.

Westerhold, T., et al., 2020. An astronomically dated record of Earth's climate and its predictability over the last 66 million years. Science 369, 1383.

Wickman, F.E., 1948. A clue to the age of certain marine sediments. J. Geol. 56 (1), 61–66.

Wilkens, R.H., Dickens, G.R., Tian, J., Backman, J., The Expedition 320/321 Scientists, 2013. Data report: revised composite depth scales for Sites U1336, U1337, and U1338. In: Pälike, H., Lyle, M., Nishi, H., Raffi, I., Gamage, K., Klaus, A. (Eds.), The Expedition 320/321 Scientists. Proceedings of the Integrated Ocean Drilling Program, Volume 320/321.

Yu, Z.J., Colin, C., Meynadier, L., Douville, E., Dapoigny, A., Reverdin, G., Wu, Q., Wan, S., Song, L., Xu, Z., Bassinot, F., 2017. Seasonal variations in dissolved neodymium isotope composition in the Bay of Bengal. Earth Planet. Sci. Letters 479, 310–321.

Zachos, J.C., Berggren, W.A., Aubry, M.-P., Mackensen, A., 1992. Isotopic and trace element geochemistry of Eocene and Oligocene foraminifers from Site 748, Kerguelen Plateau. In: Proceedings of the Ocean Drilling Program, Scientific Result, 120, pp. 839–854.

Zachos, J.C., Opdyke, B.N., Quinn, T.M., Jones, C.E., Halliday, A.N., 1999. Early Cenozoic glaciation, Antarctic weathering, and seawater $^{87}Sr/^{86}Sr$: is there a link? Chem. Geol. 161, 165–180.